Review of Guidance Techniques for Landing on Small Bodies[☆]

Pedro Simplício[a,*], Andrés Marcos[a], Eric Joffre[b], Mattia Zamaro[b], Nuno Silva[b]

[a] *University of Bristol, Queen's Building, University Walk, Bristol BS8 1TR, UK*
[b] *Airbus Defence and Space Ltd, Gunnels Wood Road, Stevenage SG1 2AS, UK*

Abstract

A renewed scientific interest has been growing in the exploration of small asteroids in addition to larger planetary bodies such as Mars, since their weaker gravitational field makes them more easily accessible. However, such exploratory missions are very challenging from an engineering perspective, particularly when striving for optimal propellant consumption. This is mostly due to the perturbed and poorly known characteristics of small planetary bodies but also, as shown by the European Rosetta mission, to the long-time degradation of spacecraft subsystems. In order to address this challenge, it has been long recognised the need for robust descent algorithms.

However, Space guidance and control communities have different understandings, restricting the integration of scientific advances and even constraining their capabilities. To incite such an integration and guide engineers in the development of planetary descent algorithms, this survey gathers state-of-practice guidance and control techniques and presents them in an instructive fashion. In addition, it clarifies and reconciles different concepts from both guidance and control perspectives. The survey and reconciliation of concepts then lead to the identification of an underlying parametric generalisation of guidance techniques, suitable for the application of systematic optimisation tools. Albeit simple, this

[☆]This work is funded by the UK Space Agency through a 2016 NSTP-2 Space Technology Fast Track grant entitled "Robust and Nonlinear Guidance and Control for Landing on Small Bodies". Mr. Simplício is also the recipient of a Doctoral Training Partnership award by the Engineering and Physical Sciences Research Council.

[*]Corresponding author
Email address: pedro.simplicio@bristol.ac.uk (Pedro Simplício)
URL: www.tasc-group.com (Technology for AeroSpace Control Lab.)

structural identification is very important as the latter tools have shown great promise and have already been employed, for example, for Rosetta's critical control update. Finally, special emphasis is placed on the robustness of those techniques against uncertainties.

Keywords: Optimal guidance, Robust control, Planetary descent

1. Introduction

Space Sample Return (SR) missions have a record of revolutionising planetary science. For example, in 2012, new chemical analyses carried out by the University of Chicago on the lunar material collected by Apollo 14 fifty years earlier have brought new elements to the disputed question of the origin of the Moon, casting a new doubt on the most widely accepted "Giant Impact" hypothesis (Zhang et al., 2012). In order to facilitate the science, all Space exploration missions require a high level of technological development. And even from the beginnings of this endeavour, the technology support ranged from the manned US missions to the Moon of the Apollo program (the first missions to return extraterrestrial samples) to the Soviet Luna missions (the first to do so relying solely on advanced robotics). More recently, technological advances have enabled sample return missions from farther celestial bodies: NASA's Stardust (Bhaskaran et al., 2004) returned cometary dust in 2006 and JAXA's Hayabusa (Yoshimitsu et al., 2009) returned microscopic grains of asteroid material in 2010.

In addition to the exploration of larger planetary bodies such as Mars, small asteroids are among the candidates for future SR missions since their weaker gravitational field makes them more easily accessible. In particular, the Martian moons are receiving significant attention from the international community, not only because of the wide scientific interest to solve the unknowns surrounding their formation, but also as technological precursors for future manned and unmanned exploration missions targeting the Martian System (Barraclough et al., 2014).

In order to succeed in these upcoming exploratory missions, descent and landing (D&L) on the target planet or asteroid represents one of the most

critical phases from an engineering perspective, especially if the natural dynamics in the vicinity of the target body is exploited to alleviate tight propellant consumption requirements. This is because small planetary bodies are typically characterised by highly irregular and poorly known shapes, which render their physical environment extremely uncertain and variable. Moreover, due to the interplanetary distances involved, fully autonomous guidance, navigation and control algorithms are required to cope with communication delays and spacecraft subsystems degradation, as demonstrated by the European Rosetta mission (Falcoz et al., 2015).

As part of the UK Space Agency National Space Technology Programme (NSTP-2) Fast Track call in 2015, the University of Bristol and Airbus Defence and Space were awarded the project entitled "Robust Nonlinear Guidance and Control for Landing on Small Bodies", with the aim to investigate the application of advanced robust control techniques for the design and optimisation of D&L trajectories on small planetary bodies. Special attention was given to approaches well-oriented towards the industrial state-of-practice, where the application of legacy knowledge is fundamental. Although a generic framework for D&L on these bodies was pursued, the project focused on the Martian moon Phobos as an illustrative case of the implications of the proposed strategies on system design and operation (for a future interplanetary SR mission). This article provides the survey on the state-of-practice on guidance techniques for D&L that was the foundation to the subsequent technological developments performed in the study (Simplício et al., 2018a,b).

The presented techniques cover applications to both small asteroids and larger planetary bodies, and it is noted that, while strategies for each have been developed rather independently, much insight can be gained by examining their joint potential. Hence, in contrast to other surveys in this domain, e.g. (Hawkins et al., 2012; Guo et al., 2013), the scope of the present one is much ampler and techniques are compared in an implementation-oriented manner. For each category, relevant Space missions are presented and guidance laws are described. In addition, emphasis is placed on a parametric description of the algorithms, which

is valuable for systematic optimisation, as well as on practical implementation issues, such as the impact of uncertainties and inaccuracies (e.g., relative to the knowledge of gravitational fields) that can lead to performance or mission loss if not addressed.

The survey is organised as follows: Sec. 2 provides an introductory background to the rest of the document including the formal definition of the planetary descent problem, Sec. 3 presents and describes the most relevant open and closed-loop guidance techniques (also known as implicit and explicit techniques) and Sec. 4 elaborates on practical issues identified throughout the survey.

2. Preliminaries on Planetary Descent

This section provides an introductory background to support the presentation and understanding of the guidance techniques reviewed throughout the rest of the article. This background begins with the mathematical formulation of the planetary descent problem in Sec. 2.1 and it is followed by a discussion on candidate guidance and control architectures in Sec. 2.2. It concludes with a brief review of relevant Space missions in Sec. 2.3 and of the applicability to a landing on Phobos in Sec. 2.4.

2.1. Mathematical problem formulation

The planetary descent configuration towards a target asteroid or planet is depicted in Fig. 1 for planar motion but without loss of generality. It describes a spacecraft approaching a moving (small) body target subject to the influence of another (large) body, i.e., the so-called two-body problem. For this problem, it is assumed that the spacecraft has a dedicated attitude control system, therefore attitude and translational dynamics are considered independent. Coupling effects are then considered at actuator level (see Sec. 2.2).

The position and velocity of the target in Fig. 1, $\mathbf{r}_T(t) \in \mathbb{R}^3$ and $\mathbf{v}_T(t) \in \mathbb{R}^3$, are described as follows:

$$\begin{aligned} \dot{\mathbf{r}}_T(t) &= \mathbf{v}_T(t) \\ \dot{\mathbf{v}}_T(t) &= \mathbf{g}_T(\mathbf{r}_T) \end{aligned} \tag{1}$$

where $\mathbf{g}_T(\mathbf{r}_T) \in \mathbb{R}^3$ is the gravitational acceleration acting on the target, which is generically expressed as a partial derivative of the potential gravity of the main body. In addition, $r_T(t) = ||\mathbf{r}_T(t)||$ and $v_T(t) = ||\mathbf{v}_T(t)||$.

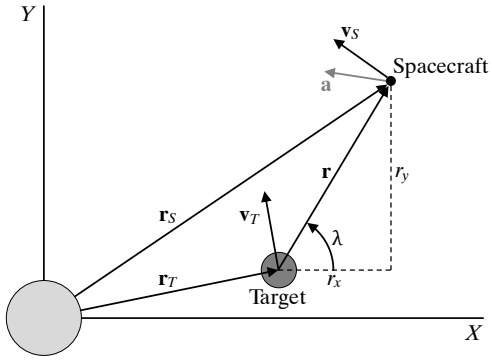

Figure 1: Problem geometry

Similarly, the position and velocity of the impactor or lander spacecraft in the same frame, $\mathbf{r}_S(t) \in \mathbb{R}^3$ with $r_S(t) = ||\mathbf{r}_S(t)||$, and $\mathbf{v}_S(t) \in \mathbb{R}^3$ with $v_S(t) = ||\mathbf{v}_S(t)||$, are modelled as (Battin, 1987):

$$\begin{aligned} \dot{\mathbf{r}}_S(t) &= \mathbf{v}_S(t) \\ \dot{\mathbf{v}}_S(t) &= \mathbf{g}_S(\mathbf{r}_T, \mathbf{r}_S) + \mathbf{a}(t) + \mathbf{p}(t) \end{aligned} \tag{2}$$

where $\mathbf{g}_S(\mathbf{r}_T, \mathbf{r}_S) \in \mathbb{R}^3$ is the gravitational acceleration felt by the spacecraft due to the main and target bodies, $\mathbf{a}(t) \in \mathbb{R}^3$ is the control acceleration provided by the spacecraft thrusters and $\mathbf{p}(t) \in \mathbb{R}^3$ represents any external perturbations (e.g., third-body perturbations) and unknowns.

Defining relative position as $\mathbf{r}(t) = \mathbf{r}_S(t) - \mathbf{r}_T(t)$ and relative velocity as $\mathbf{v}(t) = \mathbf{v}_S(t) - \mathbf{v}_T(t)$, the relative motion between spacecraft and target is expressed as:

$$\begin{aligned} \dot{\mathbf{r}}(t) &= \mathbf{v}(t) \\ \dot{\mathbf{v}}(t) &= \mathbf{g}(\mathbf{r}_T, \mathbf{r}_S) + \mathbf{a}(t) + \mathbf{p}(t) \end{aligned} \tag{3}$$

where:

$$\mathbf{g}(\mathbf{r}_T, \mathbf{r}_S) = \mathbf{g}_S(\mathbf{r}_T, \mathbf{r}_S) - \mathbf{g}_T(\mathbf{r}_T) \tag{4}$$

is the apparent gravitational acceleration. The closing velocity of the spacecraft is defined as $V_c(t) = -||\mathbf{v}(t)||$. Moreover, $\mathbf{g}(\mathbf{r}_T, \mathbf{r}_S)$ can be computed with different levels of accuracy (e.g., assuming Keplerian forces only or including detailed representations of the inhomogeneity of bodies via gravity harmonics), with all the inaccuracies contained in $\mathbf{p}(t)$. Also, note that it is important that non-inertial effects are accounted for in $\mathbf{g}(\mathbf{r}_T, \mathbf{r}_S)$ when the frame of Fig. 1 is rotating with the system.

Following the definitions above, the **descent guidance problem** is defined as: Find the acceleration law $\mathbf{a}(t)$ between $t = t_0$ and $t = t_f$ that

- Brings the relative states from the terminal boundary conditions $\mathbf{r}(t_0) = \mathbf{r}_0$ and $\mathbf{v}(t_0) = \mathbf{v}_0$ to the final conditions $\mathbf{r}(t_f) = \mathbf{r}_f$ and $\mathbf{v}(t_f) = \mathbf{v}_f$;
- Copes with the effect of external perturbations $\mathbf{p}(t)$ and uncertainties.

Two additional important concepts to describe the D&L problem that must be introduced now are the duration from a given instance of time t until the end of the manoeuvre, known as time-to-go, $t_{\text{go}}(t) = t_f - t$, and the line-of-sight (LOS) vector $\mathbf{\Lambda}(t) \in \mathbb{R}^3$, which is the direction from target to spacecraft (Hawkins et al., 2010) and is given by:

$$\mathbf{\Lambda}(t) = \frac{\mathbf{r}(t)}{r(t)} \tag{5}$$

For the planar illustration of Fig. 1, the LOS is represented by a single angle:

$$\lambda(t) = \arctan\frac{r_y(t)}{r_x(t)}, \qquad \dot{\lambda}(t) = \frac{r_x(t)\dot{r}_y(t) + r_y(t)\dot{r}_x(t)}{r^2(t)} \tag{6}$$

and, in this case:

$$\mathbf{\Lambda}(t) = \begin{bmatrix} \cos\lambda(t) \\ \sin\lambda(t) \end{bmatrix}, \qquad \dot{\mathbf{\Lambda}}(t) = \dot{\lambda}(t) \begin{bmatrix} -\sin\lambda(t) \\ \cos\lambda(t) \end{bmatrix} \tag{7}$$

In addition, and specially important to reconcile the diverse guidance laws, the concept of zero-effort errors that was first defined in (Ebrahimi et al., 2008) must be introduced:

- Zero-effort-miss (ZEM) is the position error at the end-of-mission if no corrective manoeuvres are made after time t:

$$\mathbf{ZEM}(t) = \mathbf{r}_f - \mathbf{r}(t_f) \mid \mathbf{a}(\tau) = 0 \; \forall \; \tau \in [t, t_f] \tag{8}$$

- Zero-effort-velocity (ZEV) is the velocity error at the end-of-mission if no corrective manoeuvres are made after time t:

$$\mathbf{ZEV}(t) = \mathbf{v}_f - \mathbf{v}(t_f) \mid \mathbf{a}(\tau) = 0 \; \forall \; \tau \in [t, t_f] \tag{9}$$

Position and velocity can be propagated using (3) in the absence of corrective manoeuvres, hence the ZEM and ZEV equations become:

$$\begin{aligned} \mathbf{ZEM}(t) &= \mathbf{r}_f - \left[\mathbf{r}(t) + (t_f - t)\mathbf{v}(t) + \int_t^{t_f} (t_f - \tau)\mathbf{g}(\tau)\, \mathrm{d}\tau\right] \\ \mathbf{ZEV}(t) &= \mathbf{v}_f - \left[\mathbf{v}(t) + \int_t^{t_f} \mathbf{g}(\tau)\, \mathrm{d}\tau\right] \end{aligned} \tag{10}$$

To obtain these analytical expressions for ZEM and ZEV, the apparent acceleration is typically assumed to be known as an explicit function $\mathbf{g}(t)$ of time. However, as the acceleration is more generally given as a function of position (4), the computation of ZEM and ZEV has to be approximated or performed numerically. An overview of methods for this computation is provided in Sec. 4.2.

For the development of guidance laws, spacecraft mass $m(t)$ is often also assumed constant while the control acceleration is assumed unconstrained. These approximations can be compensated by an inner control loop (see Sec. 2.2). On the other hand, for purposes of detailed dynamical simulations, the actual spacecraft acceleration results from:

$$\mathbf{a}(t) = \frac{\mathbf{T}_\mathrm{c}(t)}{m(t)} \tag{11}$$

in which the available thrust force $\mathbf{T}_\mathrm{c}(t) \in \mathbb{R}^3$ is bounded as follows:

$$0 \leq \rho_1 \leq \|\mathbf{T}_\mathrm{c}(t)\| \leq \rho_2 \tag{12}$$

2.2. Guidance and control architectures

Arising from different domains in Control Theory (optimal versus robust), and guidance versus control understanding in Space Mission Analysis, different terms are found in the literature on planetary descent techniques. Thus, this section clarifies key concepts before proceeding with the survey. This clarification is mostly supported by the two generic block diagrams depicted in Fig. 2.

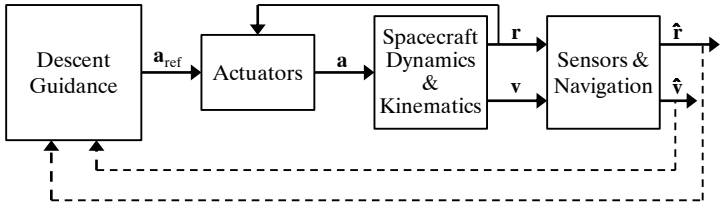

(a) Uncompensated guidance

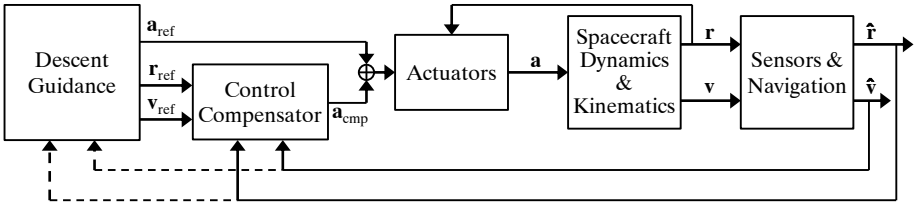

(b) Compensated guidance

Figure 2: Guidance and control architectures (dashed lines represent flow of information for closed-loop guidance techniques)

Referring to Fig. 2, the Spacecraft Dynamics & Kinematics (SDK) block represents essentially the simulation of the relative translational motion (3). The complexity of this simulation depends on that of (4), since $\mathbf{g}(\mathbf{r}_T, \mathbf{r}_S)$ can be highly nonlinear for very accurate gravitational models.

The SDK block is fed by the spacecraft Actuators, which are commanded by the guidance and/or control systems. The actuators account for realisation errors of the spacecraft thrusters due to mounting errors and gas-dynamics properties, as well as for maximum thruster capability (12) and limited authority (if also employed for position-dependent attitude control).

Furthermore, the outputs of the SDK block are measured and filtered by the Sensors & Navigation subsystem before being used for guidance/control. This process introduces noise and quantisation errors in the relative position and velocity estimates, $\hat{\mathbf{r}}(t)$ and $\hat{\mathbf{v}}(t)$.

Focusing now on Fig. 2a, two different guidance paradigms for planetary descent can be defined. The first one is the so-called *open-loop guidance* (also known as *implicit guidance*) which refers to the case when a complete reference trajectory $\mathbf{r}_{\text{ref}}(t), \mathbf{v}_{\text{ref}}(t)$ and thruster profile $\mathbf{a}_{\text{ref}}(t)$ are designed before the

descent, stored and remain unchanged throughout the manoeuvre. In the Space domain, these references are designed based on Mission Analysis considerations. The second paradigm is then called *closed-loop guidance* (also known as *explicit guidance*) when the reference thruster profile $\mathbf{a}_{\text{ref}}(t)$ is computed in real-time throughout the descent in order to correct the trajectory based on onboard measurements, $\hat{\mathbf{r}}(t)$ and $\hat{\mathbf{v}}(t)$. This feedback of information is represented with dashed lines in the figure. In this case, the Descent Guidance subsystem might also be responsible for the computation of auxiliary variables such as the LOS (5) or zero-effort errors (10).

In addition to the Descent Guidance subsystem, a Control Compensator can be included, as illustrated in Fig. 2b, to further alleviate trajectory errors. This alleviation is achieved by introducing an additional acceleration vector command $\mathbf{a}_{\text{cmp}}(t)$ that compensates for deviations between reference trajectory and measured states. This is however outside the scope of this survey and thus the remainder of the paper focuses on Descent Guidance techniques and their implementation. But as an example of control compensator design, the reader is referred to (Simplício et al., 2018a), where an application to the scenario of a landing on Phobos is presented. In this reference, deviations between reference and measured states were modelled as linear orbital perturbations (Battin, 1987) and control synthesis was performed using robust control techniques. The internal structure adopted and an example of the simulation results obtained with this approach are depicted in Fig. 3.

2.3. Missions and categories

In recent years, a renewed interest in small planetary bodies has led to several studies and missions. There are mainly two different purposes behind these studies and missions. On the one hand, there is the exploitation of hypervelocity impact with a spacecraft as a mitigation strategy against objects on a course for potential collision with Earth. Notable examples of this type of missions include NASA's Deep Impact Spacecraft (Kubitschek, 2003), which successfully hit comet Tempel 1 on July 2005 at 10 km/s (Fig. 4), and ESA's Asteroid Impact Mission (Ferrari et al., 2015), undergoing preliminary design phase but

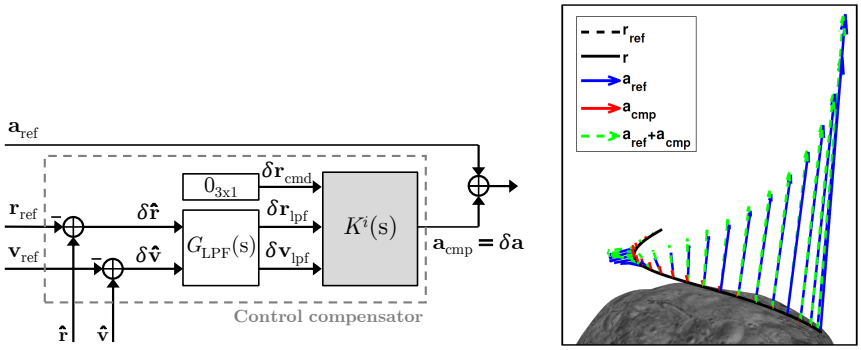

(a) Internal architecture (b) High-fidelity simulation

Figure 3: Example of control compensation

planned to rendezvous with the Didymos binary asteroid system around 2021 (and observe closely the collision with an impactor a few months after).

On the other hand, there is also the interest of touch-and-go or landing on planetary bodies instead of impacting, as the scientific return in general is much higher. Successful missions in this category include NASA's Stardust (Bhaskaran et al., 2004), launched in 1999 and the first SR mission to collect comet and cosmic dust samples, JAXA's Hayabusa (Yoshimitsu et al., 2009), a mission that landed on Itokawa asteroid on November 2005 returning to Earth five years after, and ESA's Rosetta (Geurts et al., 2014), which performed a rendezvous with comet Churyumov-Gerasimenko and delivered a lander for on-site analysis on November 2014 (Fig. 5). In addition, NASA has launched OSIRIS-REx (Williams et al., 2018) in September 2016, an SR spacecraft that will reach the near-Earth asteroid Bennu, while ESA is also studying the feasibility of an SR mission to Phobos (Barraclough et al., 2014), one of Mars' moons. And more recently, JAXA's Hayabusa-2 (Kuninaka & Hayabusa-2 team, 2015) successfully delivered in September 2018 two small landers on Ryugu (taking advantage of the asteroid's weak gravitational field) and is scheduled to land another two, as well as to obtain and return samples using an explosive penetrator.

For both interception and landing on small bodies, autonomous systems are mandatory to guide spacecraft through very uncertain operational environments

while coping with long communication delays with Earth. The earliest known method is inspired by the missile interception problem. It is known as proportional navigation guidance (PNG) and introduced in (Zarchan, 1994), where a method of augmenting it when the target acceleration is known or can be assumed is also provided. In addition, guidance using predictive manoeuvres based on linear orbital perturbation theory (Battin, 1987) is proven possible and complemented with PNG in (Gil-Fernandez et al., 2008).

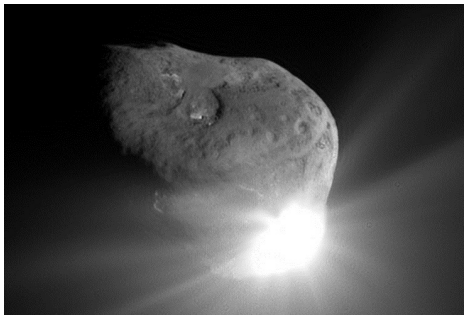

Figure 4: Image taken by Deep Impact's flyby craft after the collision of its impactor with comet Tempel 1 [Credits: *NASA/JPL-Caltech/UMD*]

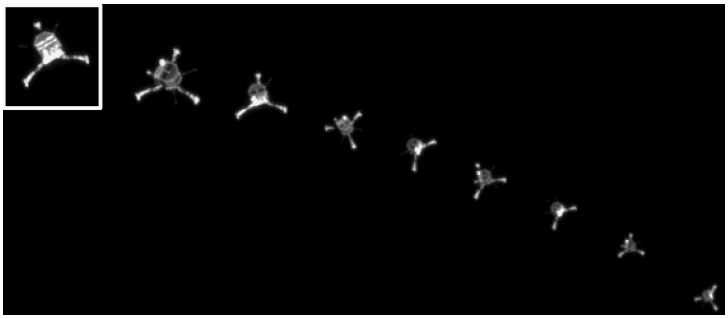

Figure 5: Series of images captured by Rosetta's camera as its lander descended to comet Churyumov-Gerasimenko [Credits: *ESA/Rosetta/MPS*]

However, most of the work on traditional closed-loop guidance for small bodies recasts the problem as optimal feedback control with terminal constraints only (i.e., with no path constraints), which is solved with the Pontryagin maximum principle in (Battin, 1987) or through calculus of variations in (D'Souza, 1997). This type of laws, known as optimal guidance laws (OGLs), has been continuously

developed for different terminal boundary conditions (e.g., constrained velocity, free velocity, constrained intercept-angle, etc.) and also related to the classical PNG laws (see, for example, (Hawkins et al., 2011)).

Additionally, and due to the highly uncertain character of the operational environments, OGLs have been recently augmented with nonlinear terms based on sliding mode control (SMC) theory in order to increase their robustness in the presence of inaccurate measurements and unmodelled dynamics (Ebrahimi et al., 2008). Because of the improved robustness that can be achieved, this research topic has been evolving and applied to different scenarios in the past few years (Furfaro et al., 2011, 2013b).

In parallel, different descent techniques have been developed and applied for the exploration of larger bodies, such as the Moon and Mars. These approaches are not as demanding as for the asteroid intercept problem since curvature of the planet can often be neglected and its gravity field is relatively uniform and well known. Hence, the first-generation of Mars probes that successfully reached its surface, from NASA's Viking 1 in 1976 to Phoenix in 2008 (Fig. 6), relied on an unguided descent phase. As a consequence, these systems generated a landing uncertainty ellipse in the order of 500 km by 100 km (Li & Jiang, 2014).

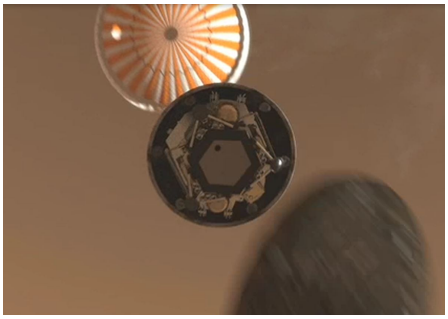

Figure 6: Artist's concept of Phoenix Mars lander after jettisoning its heat shield before firing its thrusters [Credits: *NASA/JPL-Caltech/UA*]

When the mission has to satisfy more stringent requirements such as very high landing accuracy or crew safety (in the case of manned missions), then the strategies used are generally based by solving a trajectory-generation problem with both terminal and path constraints. This type of approach begun with

the Apollo program and continues with the next-generation Mars landers (for which the capability of pinpoint landing the spacecraft in hazardous sites with high scientific value is mandatory, thus requiring an uncertainty ellipse down to 100 m (Li & Jiang, 2014)), and is also used on Earth by reusable vertical take-off vertical landing (VTVL) launch vehicles as those from SpaceX and Blue Origin (Blackmore, 2016).

The aforementioned problem is typically nonlinear and challenging to solve and, until the past decade, its application was only feasible in an offline setting (where open-loop trajectories are designed on the ground with powerful computers). To simplify the problem, during the Apollo program, an acceleration profile that is a quadratic function of time (Klumpp, 1974) was chosen. This profile was not optimal in the sense that no cost function was optimised, but the quadratic coefficients could be computed analytically from the terminal boundary conditions for a pre-specified descent duration. This approach was modified for the NASA's Mars Science Laboratory (MSL) Curiosity in 2011, by adding a line-search over the powered descent duration so as to minimise propellant consumption (Ploen et al., 2006; Wong et al., 2006). In addition to these simplifications and extensions, augmenting the polynomial order of an open-loop guidance law renders the computation of the coefficients under-determined and thus, this allows choosing them so as to optimise a desired cost function.

A plethora of optimisation algorithms can be applied to solve this augmented-coefficient optimisation problem offline while enforcing different path constraints (such as minimum altitude or maximum actuation). However, the increase of computational power available onboard in recent years has enabled representative solutions to be determined and applied in a closed-loop fashion, leading to a paradigm shift known as *Computational Guidance and Control* (Special Issue on Computational Guidance and Control, 2017). This is supplemented by specific semi-analytical algorithms (e.g., (Lunghi et al., 2013, 2014)) or by further mathematical developments (in the domain of convex optimisation and pseudospectral methods, summarised in Sec. 3.3).

Nonetheless, methods for extraterrestrial autonomous pinpoint landing have

very little heritage and have only recently been demonstrated with NASA's reusable VTVL platform Xombie (Fig. 7), which uses a vision system to determine its location and the guidance for fuel-optimal large diverts (G-FOLD) algorithm to optimally fly to the landing site (Açikmeşe et al., 2013; Scharf et al., 2014).

Figure 7: Photo of NASA's reusable VTVL platform Xombie demonstrating Mars-like descent and pinpoint landing [Credits: *NASA/Tom Tschida*]

2.4. Applicability to a landing on Phobos

Although developed in parallel, the solutions introduced in Sec. 2.3 have the potential to complement more traditional techniques targeting small bodies such as Phobos which, due to their irregular shapes and mass distributions (Fig. 8a), are characterised by very variable and uncertain gravitational fields, with complex orbits stable only in certain regions (Lara & Scheeres, 2003).

Moreover, in the case of Phobos, as this moon is very small and close to Mars, the boundary of the planet's sphere of influence lies just above Phobos' surface (Fig. 8b) and its third-body perturbation cannot be neglected.

As mentioned in Sec. 1, although a generic framework for planetary descent is pursued in this article, the scenario of a landing on Phobos is employed as an illustrative case. With this is mind, candidate guidance techniques for a landing on Phobos are exemplified throughout the next section. Here, the relative motion (3) is simulated by a high-fidelity dynamics model of the Mars-Phobos system, in which the gravity field of the planets is described by a main Keplerian term plus gravity harmonics to account for their inhomogeneity. Uncertainties and variations can also be included in the gravity field of Phobos by dispersing

its gravity harmonics coefficients. A more generic robustness comparison of guidance techniques is provided in Sec. 4.1.

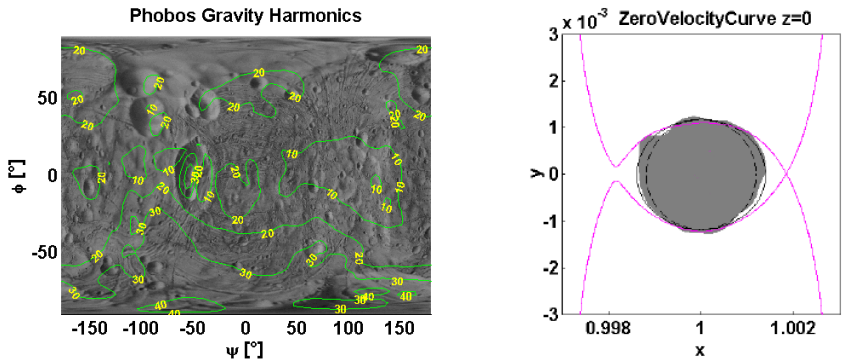

(a) Difference of gravitational acceleration between gravity harmonics and Keplerian model

(b) Mars's sphere of influence around Phobos

Figure 8: Highly inhomogeneous gravitational field in the vicinity of Phobos [Credits: *Airbus Defence and Space*]

3. Overview of Guidance Techniques

This section is dedicated to the description of the guidance techniques introduced in Sec. 2.3. They are divided in open-loop (Sec. 3.1), traditional closed-loop (Sec. 3.2) and computational closed-loop guidance (Sec. 3.3). In addition, insight on future trends of these techniques from an industrial point is given in Sec. 3.4 and an overall summary is provided in Sec. 3.5.

3.1. Open-loop guidance

Open-loop (or implicit) guidance relies on the design of a reference trajectory and thruster profile before initiating the descent. Depending on the type of profile, open-loop guidance laws can be further classified as quadratic (Sec. 3.1.1) or optimal with path constraints (Sec. 3.1.2).

3.1.1. Quadratic

As previously mentioned, for landing on larger planetary bodies where the gravity field is well known and can be assumed constant, open-loop guidance

techniques often suffice. For the Apollo program, emphasis was placed on developing computationally feasible guidance laws rather than looking for complex energy-optimal solutions. Hence, the Apollo guidance law is simply defined as a quadratic function of time (Klumpp, 1974; Wong et al., 2006):

$$\mathbf{a}(t) = \mathbf{C}_0 + \mathbf{C}_1 t + \mathbf{C}_2 t^2 \tag{13}$$

where $\mathbf{C}_i \in \mathbb{R}^3$ are coefficients to be determined. Velocity and position are obtained assuming a constant gravity field and integrating the above acceleration:

$$\mathbf{v}(t) = \mathbf{v}_0 + (\mathbf{C}_0 + \mathbf{g})\, t + \frac{1}{2}\mathbf{C}_1 t^2 + \frac{1}{3}\mathbf{C}_2 t^3 \tag{14}$$

$$\mathbf{r}(t) = \mathbf{r}_0 + \mathbf{v}_0 t + \frac{1}{2}\,(\mathbf{C}_0 + \mathbf{g})\, t^2 + \frac{1}{6}\mathbf{C}_1 t^3 + \frac{1}{12}\mathbf{C}_2 t^4 \tag{15}$$

Applying the boundary conditions at the end-of-mission ($t = t_f$) as defined in Sec. 2.1, the unknown coefficients are obtained by solving the linear system:

$$\begin{bmatrix} \mathbb{I} & t_f\mathbb{I} & t_f^2\mathbb{I} \\ t_f\mathbb{I} & \frac{t_f^2}{2}\mathbb{I} & \frac{t_f^3}{3}\mathbb{I} \\ \frac{t_f^2}{2}\mathbb{I} & \frac{t_f^3}{6}\mathbb{I} & \frac{t_f^4}{12}\mathbb{I} \end{bmatrix} \begin{bmatrix} \mathbf{C}_0 + \mathbf{g} \\ \mathbf{C}_1 \\ \mathbf{C}_2 \end{bmatrix} = \begin{bmatrix} \dot{\mathbf{v}}(t_f) \\ \mathbf{v}_f - \mathbf{v}_0 \\ \mathbf{r}_f - \mathbf{r}_0 - \mathbf{v}_0 t_f \end{bmatrix} \tag{16}$$

which is given by:

$$\begin{aligned} \mathbf{C}_0 &= \dot{\mathbf{v}}(t_f) - \mathbf{g} - \frac{6}{t_f}(\mathbf{v}_f - \mathbf{v}_0) + \frac{12}{t_f^2}(\mathbf{r}_f - \mathbf{r}_0 - \mathbf{v}_0 t_f) \\ \mathbf{C}_1 &= -\frac{6}{t_f}\dot{\mathbf{v}}(t_f) + \frac{30}{t_f^2}(\mathbf{v}_f - \mathbf{v}_0) - \frac{48}{t_f^3}(\mathbf{r}_f - \mathbf{r}_0 - \mathbf{v}_0 t_f) \\ \mathbf{C}_2 &= \frac{6}{t_f^2}\dot{\mathbf{v}}(t_f) - \frac{24}{t_f^3}(\mathbf{v}_f - \mathbf{v}_0) + \frac{36}{t_f^4}(\mathbf{r}_f - \mathbf{r}_0 - \mathbf{v}_0 t_f) \end{aligned} \tag{17}$$

In this type of guidance, the end-of-mission time (or alternatively the time-to-go, $t_{\text{go}}(t) = t_f - t$) is a free parameter that must be specified. A brief discussion on how to automatically set a reasonable time-to-go, or even determine an optimal value is provided in Sec. 4.3.

3.1.2. Optimal with path constraints

Planetary descent guidance with a direct consideration of physical state and control constraints can also be implemented in an open-loop fashion. The basis for these sophisticated implicit guidance methods is actually the quadratic

acceleration law of (13), in which all the coefficients are completely determined, but in this case augmenting its order to $N > 2$:

$$\mathbf{a}(t) = \mathbf{C}_0 + \mathbf{C}_1 t + \ldots + \mathbf{C}_N t^N \tag{18}$$

This higher order polynomial structure for the acceleration allows for significant improvements (Ploen et al., 2006; Singh et al., 2007), since the terminal linear system (16) is now under-determined:

$$\begin{bmatrix} \mathbb{I} & t_f\mathbb{I} & \ldots & t_f^N\mathbb{I} \\ t_f\mathbb{I} & \frac{t_f^2}{2}\mathbb{I} & \ldots & \frac{t_f^{N+1}}{(N+1)}\mathbb{I} \\ \frac{t_f^2}{2}\mathbb{I} & \frac{t_f^3}{6}\mathbb{I} & \ldots & \frac{t_f^{N+2}}{(N+1)(N+2)}\mathbb{I} \end{bmatrix} \begin{bmatrix} \mathbf{C}_0 + \mathbf{g} \\ \mathbf{C}_1 \\ \vdots \\ \mathbf{C}_N \end{bmatrix} = \begin{bmatrix} \dot{\mathbf{v}}(t_f) \\ \mathbf{v}_f - \mathbf{v}_0 \\ \mathbf{r}_f - \mathbf{r}_0 - \mathbf{v}_0 t_f \end{bmatrix} \tag{19}$$

Therefore, the solution of the acceleration coefficients $\mathbf{C}_i \in \mathbb{R}^3$ and of t_f can be determined so as to optimise a specified cost function (e.g., propellant consumption) while subject to the linear system (19), as well as to path state and control constraints. These may include bounded thrust force (12), admissible mass variation, subsurface flight avoidance ($r(t) \geq h_{\text{MIN}}$) or any additional position and velocity constraints (e.g., obstacle avoidance, glide-slope angle or maximum velocity) all given as generalised linear inequalities.

Depending on the formulation of the constrained optimisation problem, a plethora of solvers is available and, depending on the solver, parametric descriptions of the acceleration profile different than (18) may also be considered. For the case of Phobos, open-loop guidance laws have been designed through the following process:

1. Analysis of a set of unstable manifolds originated at libration point orbits in the Mars-Phobos system that intersect the moon;
2. Selection as initial guesses the manifolds that reach it with higher incidence angle and lower closing speed;
3. Definition of a polynomial acceleration profile aimed at bringing the final speed to zero;
4. Optimisation of the initial guesses and acceleration profile via nonlinear programming, with the objective of minimum fuel consumption.

For further details on this process, the reader is referred to (Joffre et al., 2017). To simplify the optimisation runs, an approximate model of the Mars-Phobos system (denoted MAG - Mission Analysis and Guidance) is employed. The optimal trajectory using the latter model and the result of applying the corresponding acceleration profile to a high-fidelity environment (DKE - Dynamics, Kinematics and Environment) are both depicted in Fig. 9.

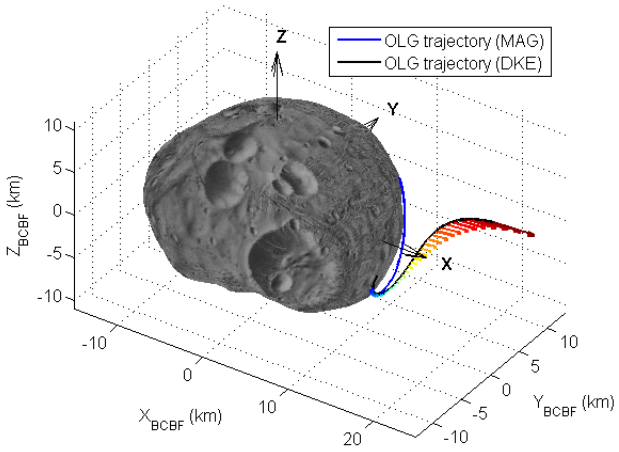

Figure 9: Phobos D&L trajectory using open-loop guidance (arrows represent magnitude and direction of acceleration commands)

In this figure, it is shown that the trajectory rapidly diverges from the optimal one (obtained with the MAG model) under the influence of a slightly different dynamics environment (DKE). This shows that, as anticipated in Sec. 2.3, open-loop command profiles do not typically yield suitable standalone D&L guidance strategies for bodies with complex and perturbed gravity fields.

3.2. Traditional closed-loop guidance

In traditional closed-loop guidance, the thruster profile is computed as a closed-form solution to actively correct the descent trajectory. Depending on the type of solution, guidance laws can be further classified as proportional (Sec. 3.2.1), predictive and hybrid (Sec. 3.2.2), optimal without path constraints (Sec. 3.2.3) and nonlinear robust (Sec. 3.2.4).

3.2.1. Proportional

The earliest known guidance strategy for the interception of small bodies is inspired by the missile interception problem and is known as proportional navigation guidance (PNG). PNG laws and their most basic variations are introduced in (Zarchan, 1994) and thoroughly described in (Hawkins et al., 2012; Guo et al., 2013). The principle of PNG is to drive the LOS rate to zero by applying a proportional acceleration perpendicularly to the LOS direction:

$$\mathbf{a}(t) = nV_c(t)\dot{\mathbf{\Lambda}}(t) \tag{20}$$

where n is the effective navigation ratio, a tunable parameter typically chosen between 3 and 5. Smaller values result in reduced propellant consumption whereas larger values are adopted for improved robustness at the expense of higher acceleration commands. For the planar case, i.e., equation (7), the acceleration becomes:

$$\mathbf{a}(t) = nV_c(t)\dot{\lambda}(t) \begin{bmatrix} -\sin\lambda(t) \\ \cos\lambda(t) \end{bmatrix} \tag{21}$$

This guidance law does not require the target or spacecraft accelerations to be zero, but its performance is improved if the contribution of the gravitational environment is deducted. This results in the augmented PNG (APNG) law:

$$\mathbf{a}(t) = nV_c(t)\dot{\mathbf{\Lambda}}(t) - \frac{n}{2}\mathbf{g}_\perp(t) \tag{22}$$

where again $\mathbf{g}_\perp(t)$ are the components of apparent gravity perpendicular to the LOS. For the planar case, the APNG law simplifies into:

$$\mathbf{a}(t) = n\left(V_c(t)\dot{\lambda}(t) - \frac{1}{2}g_\perp(t)\right) \begin{bmatrix} -\sin\lambda(t) \\ \cos\lambda(t) \end{bmatrix} \tag{23}$$

with $g_\perp(t) = \begin{bmatrix} -\sin\lambda(t) & \cos\lambda(t) \end{bmatrix} \mathbf{g}(t)$. Moreover, employing the definitions of time-to-go and zero-effort-miss (10), it can be shown that the APNG law becomes:

$$\mathbf{a}(t) = \frac{n}{t_{\text{go}}^2(t)}\mathbf{ZEM}(t) \tag{24}$$

where the time-to-go cannot be controlled, but is computed as $t_{\text{go}}(t) = r(t)/V_c(t)$.

In (Kim et al., 1998), an adaptation of the APNG law known as biased PNG (BPNG) is also explored. This biased law allows to constrain the impact (final) LOS angle to λ_f resulting in:

$$\mathbf{a}(t) = \left(4V_c(t)\dot{\lambda}(t) - g_\perp(t) + 2V_c(t)\frac{\lambda(t) - \lambda_f}{t_{\text{go}}(t)}\right)\begin{bmatrix} -\sin\lambda(t) \\ \cos\lambda(t) \end{bmatrix} \tag{25}$$

Finally, for thrusters with no continuous throttling ability (only on-off), PNG laws have to be applied using a discrete scheme, through a pulse-modulation method (Wie, 2008). In this case, the guidance is known as pulsed PNG (PPNG).

3.2.2. Predictive and hybrid

A more propellant-efficient method to perform pulsed navigation is to compute impulsive velocity corrections, which eliminate the predicted end-of-mission error by using linearised orbital perturbation theory (Battin, 1987) and apply them only at pre-scheduled firing times $\mathcal{T}_p$. Acceleration commands are provided as:

$$\mathbf{a}(t) = \begin{cases} \dfrac{\Delta\mathbf{v}_S(t)}{\Delta t_p}, & \text{for } t \in \mathcal{T}_p \\ 0, & \text{otherwise} \end{cases} \tag{26}$$

where Δt_p is the duration of the correction and $\mathcal{T}_p$ is the set of pre-scheduled times. This method is designated predictive navigation and it is assessed in (Gil-Fernandez et al., 2008) and detailed in (Hawkins et al., 2010).

If full information on the relative position and velocity vectors is available, then the guidance is known as predictive impulsive (PI) and, recalling (5), the velocity correction to be applied is:

$$\Delta\mathbf{v}_S(t) = V_c(t)\breve{\mathbf{\Lambda}}(t_f) - \mathbf{v}(t) = V_c(t)\frac{\breve{\mathbf{r}}(t_f)}{\breve{r}(t_f)} - \mathbf{v}(t) \tag{27}$$

where $\breve{}$ indicates a predicted term. The term $\breve{\mathbf{r}}(t_f)$ is the predicted relative end-of-mission position, propagated from time t through a linearised time-varying state transition matrix (STM) yielding:

$$\breve{\mathbf{r}}(t_f) \approx \left(\mathbb{I} + \frac{1}{2}G(t)t_{\text{go}}^2(t)\right)\mathbf{r}(t) \tag{28}$$

where $\mathbb{I}$ is the identity operator and $G(t)$ is the gravity Jacobian along the reference orbit (Battin, 1987):

$$G(t) = \left. \frac{\partial \, \mathbf{g}(\mathbf{r}, t)}{\partial \, \mathbf{r}(t)} \right|_{\mathbf{r}(t)=\mathbf{r}_{\mathrm{ref}}(t)} \tag{29}$$

In the case that measurements or estimates of the relative states are not available, then the kinematics of the system must be estimated using for example optical LOS information:

$$\begin{aligned} \mathbf{r}(t) &= V_c(t) t_{\mathrm{go}}(t) \mathbf{\Lambda}(t) \\ \mathbf{v}(t) &= V_c(t) t_{\mathrm{go}}(t) \dot{\mathbf{\Lambda}}(t) + V_c(t) \mathbf{\Lambda}(t) \end{aligned} \tag{30}$$

In this case, the guidance law is known as kinematic impulsive (KI) and it is obtained by substituting (30) into the velocity correction (27):

$$\Delta \mathbf{v}_S(t) = V_c(t) \frac{\breve{\mathbf{r}}(t_f)}{\breve{r}(t_f)} - V_c(t) \left(t_{\mathrm{go}}(t) \dot{\mathbf{\Lambda}}(t) + \mathbf{\Lambda}(t) \right) \tag{31}$$

as well as into the predicted end-of-mission position (28):

$$\breve{\mathbf{r}}(t_f) = V_c(t) t_{\mathrm{go}}(t) \left(\mathbb{I} + \frac{1}{2} G(t) t_{\mathrm{go}}^2(t) \right) \mathbf{\Lambda}(t) \tag{32}$$

With respect to the firing times $\mathcal{T}_p$ of the thrusters, earlier firings will lead to less propellant consumption because of the propagated corrective effect – even if the sensed information is less accurate when the spacecraft is away from the target. On the other hand, in these cases, performance tends to degrade near the end-of-mission as further gravity linearisations cause increasing approximation errors. For this reason, a hybrid guidance scheme is typically adopted, which implements mid-course predictive corrections and then switches to terminal PNG (Gil-Fernandez et al., 2008).

3.2.3. Optimal without path constraints

Most of the work on guidance laws for small bodies recasts the problem as optimal feedback control, resulting in a class known as optimal guidance laws (OGLs). This problem can be solved using either the Pontryagin maximum principle (Battin, 1987) or calculus of variations (D'Souza, 1997), although these derivations assume $\mathbf{r}_f = \mathbf{v}_f = 0$. The OGLs have been generalised in (Hawkins et al., 2011) as described in this section.

The objective of the optimal control problem is to find the acceleration profile $\mathbf{a}(t)$ that minimises the actuation effort, formulated as the cost function:

$$J(\mathbf{a}(t)) = \int_t^{t_f} L(\mathbf{x}(\tau), \mathbf{a}(\tau))\, \mathrm{d}\tau = \int_t^{t_f} \frac{1}{2}\mathbf{a}^{\mathrm{T}}(\tau)\mathbf{a}(\tau)\, \mathrm{d}\tau \tag{33}$$

subject to the dynamics of the system (3):

$$\dot{\mathbf{x}}(t) = \mathbf{f}\left(\mathbf{x}(t), \mathbf{a}(t)\right) \Leftrightarrow \begin{bmatrix} \dot{\mathbf{r}}(t) \\ \dot{\mathbf{v}}(t) \end{bmatrix} = \begin{bmatrix} \mathbf{v}(t) \\ \mathbf{g}(\mathbf{r}_T, \mathbf{r}_S) + \mathbf{a}(t) \end{bmatrix} \tag{34}$$

and the terminal boundary conditions introduced in Sec. 2.1.

In order to solve this problem, it is convenient to define position and velocity co-states, $\mathbf{p}_r(t) \in \mathbb{R}^3$ and $\mathbf{p}_v(t) \in \mathbb{R}^3$, which are described by:

$$\begin{aligned} \begin{bmatrix} \dot{\mathbf{p}}_r(t) & \dot{\mathbf{p}}_v(t) \end{bmatrix} &= -\begin{bmatrix} \mathbf{p}_r(t) & \mathbf{p}_v(t) \end{bmatrix} \frac{\partial\, \mathbf{f}(\mathbf{x}(t), \mathbf{a}(t))}{\partial\, \mathbf{x}(t)} + \frac{\partial\, L(\mathbf{x}(t), \mathbf{a}(t))}{\partial\, \mathbf{x}(t)} = \\ &= -\begin{bmatrix} 0 & \mathbf{p}_r(t) \end{bmatrix} \end{aligned} \tag{35}$$

These are then solved via integration until the terminal co-states are obtained:

$$\begin{aligned} \mathbf{p}_r(t) &= \mathbf{p}_r(t_f) \\ \mathbf{p}_v(t) &= \mathbf{p}_v(t_f) + \mathbf{p}_r(t_f) t_{\mathrm{go}}(t) \end{aligned} \tag{36}$$

In addition, the Pontryagin maximum principle states that the optimal acceleration profile, minimising $J(\mathbf{a}(t))$ in (33), is the one that cancels out the Hamiltonian derivative:

$$\left.\frac{\partial\, H(\mathbf{x}(t), \mathbf{a}(t))}{\partial\, \mathbf{a}(t)}\right|_{\text{optimal}} = 0 \Rightarrow \mathbf{a}(t) = \mathbf{p}_v(t_f) + \mathbf{p}_r(t_f) t_{\mathrm{go}}(t) \tag{37}$$

maximising the Hamiltonian function $H(\mathbf{x}(t), \mathbf{a}(t))$ given by:

$$\begin{aligned} H(\mathbf{x}(t), \mathbf{a}(t)) &= \begin{bmatrix} \mathbf{p}_r(t) \\ \mathbf{p}_v(t) \end{bmatrix}^{\mathrm{T}} \mathbf{f}(\mathbf{x}(t), \mathbf{a}(t)) - L(\mathbf{x}(t), \mathbf{a}(t)) = \\ &= \begin{bmatrix} \mathbf{p}_r(t_f) & \mathbf{p}_v(t_f) + \mathbf{p}_r(t_f) t_{\mathrm{go}}(t) \end{bmatrix} \begin{bmatrix} \mathbf{v}(t) \\ \mathbf{g}(\mathbf{r}_T, \mathbf{r}_S) + \mathbf{a}(t) \end{bmatrix} - \frac{1}{2}\mathbf{a}^{\mathrm{T}}(t)\mathbf{a}(t) \end{aligned} \tag{38}$$

From (37), it is observed that the optimal acceleration law is a linear function of the time-to-go (and thus of t) that depends only on the terminal co-states.

These are determined from the terminal states by integrating the acceleration twice, exactly as was done in Sec. 3.1.1.

To obtain a closed-form solution, a constant gravity field is assumed, yielding the expression for the so-called constrained terminal velocity guidance (CTVG) law:

$$\mathbf{a}(t) = 6\frac{\mathbf{r}_f - [\mathbf{r}(t) + \mathbf{v}_f t_{\text{go}}(t)]}{t_{\text{go}}^2(t)} + 4\frac{\mathbf{v}_f - \mathbf{v}(t)}{t_{\text{go}}(t)} - \mathbf{g} \tag{39}$$

For the case when the terminal velocity is unconstrained (e.g., no soft landing is required), the corresponding co-state is zero, $\mathbf{p}_v(t_f) = 0$, and the so-called free terminal velocity guidance (FTVG) solution can be found:

$$\mathbf{a}(t) = 3\frac{\mathbf{r}_f - \mathbf{r}(t)}{t_{\text{go}}^2(t)} - 3\frac{\mathbf{v}(t)}{t_{\text{go}}(t)} - \frac{3}{2}\mathbf{g} \tag{40}$$

Furthermore, if the zero-effort equations (10) are analytically integrated for a constant gravity field, the CTVG and FTVG laws can be re-written as:

$$\mathbf{a}(t) = \frac{6}{t_{\text{go}}^2(t)}\mathbf{ZEM}(t) - \frac{2}{t_{\text{go}}(t)}\mathbf{ZEV}(t) \tag{41}$$

$$\mathbf{a}(t) = \frac{3}{t_{\text{go}}^2(t)}\mathbf{ZEM}(t) \tag{42}$$

Comparing equations (24) and (42), it is concluded that FTVG corresponds to the APNG law for a navigation ratio $n = 3$, which means that this represents the optimal value of proportional laws.

In addition, writing the CTVG and FTVG laws generically as a function of ZEM and ZEV avoids the constant gravity assumption at the expense of requiring a more accurate integration of the zero-effort errors. If such an integration is still too complex, a candidate alternative is to perform the computation with respect to a set of intermediate waypoints interpolated on a reference trajectory, as evidenced in Fig. 10, using a fixed guidance time-horizon (Joffre et al., 2017).

The latter approach has been applied to the case of Phobos using CTVG and the optimal trajectory of Fig. 9 (from the MAG model) as reference. The resulting trajectory and commanded acceleration with 14 waypoints (time-horizon $t_h = 500$ s) are illustrated in Fig. 11.

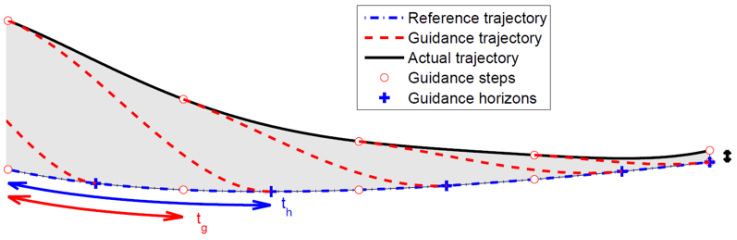

Figure 10: Illustration of closed-loop guidance with intermediate horizons

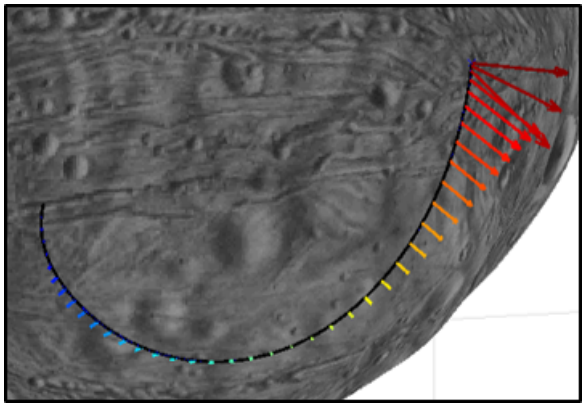

Figure 11: Phobos D&L trajectory using CTVG (arrows represent magnitude and direction of acceleration commands)

Figure 11 shows that a successful landing on Phobos can be achieved using this approach, with smooth acceleration commands and with trajectory coinciding to the reference one.

Note also that OGL laws allow to define state constraints only at terminal conditions, but not during the manoeuvre itself (path constraints). Also, they do not directly impose any kind of control constraints. This shortcoming is the main motivation for the constrained guidance strategies introduced in Sec. 3.1.2. Nevertheless, several developments of the OGLs can be found in the literature to indirectly account for specific types of constraints:

- In (Ebrahimi et al., 2008), an OGL is derived for a fixed-interval guidance manoeuvre, with a continuous firing that burns-out several seconds before touching down. It is then called optimal fixed-interval guidance law (OFIGL).

- In (Hawkins & Wie, 2011), an optimal law to control the impact (or glide-slope) angle is obtained by leaving the terminal velocity in the desired direction free and constraining the remaining components to zero. This law is called intercept-angle-control guidance (IACG) and it is shown to yield the BPNG law (25) for the case of planar motion.

- In (Guo et al., 2012), a methodology to cope with thrust and power limited engines is proposed combining the OGLs with the generation of intermediate optimal waypoints.

- In (Guo et al., 2013), the case when the landing site is not specified is tackled by indirectly incorporating the constraint $\mathbf{r}_f^{\mathrm{T}}\mathbf{r}_f = R_T^2$ as a weighted index in the cost function $J(\mathbf{a}(t))$, where R_T is the radius of the target.

- In (Zhou & Xia, 2014), a weighted term is added to the cost function $J(\mathbf{a}(t))$ to penalise trajectories that go under a certain altitude with respect to the target and even below its surface (subsurface flight).

3.2.4. Nonlinear robust

In opposition to the guidance methods presented in Sec. 3.1, the techniques from Sec. 3.2.1 to 3.2.3 do rely on closed-loop feedback control, although assuming that the parameters on which they depend are fully known. Therefore, inaccurate measurements or unmodelled dynamics can affect the results negatively. To overcome this issue, in (Ebrahimi et al., 2008) it is proposed to augment the energy-optimal laws with advancements in the field of nonlinear control. This augmentation is rooted on nonlinear sliding mode control (SMC) theory (Levant, 2007; Shtessel et al., 2014) and results in guidance algorithms that are globally stable in uncertain dynamical environments for which an upper bound of the perturbing acceleration $\mathbf{p}(t)$ is known. These algorithms are named optimal sliding guidance (OSG) and are further developed in (Furfaro et al., 2011, 2013b).

OSG laws are derived by defining a sliding surface as a linear combination of tracking (zero-effort) errors:

$$\mathbf{s}(t) = \mathbf{ZEV}(t) + \tilde{\lambda}(t)\mathbf{ZEM}(t) \tag{43}$$

where $\tilde{\lambda}(t) > 0 \; \forall \; t \in [t_0, t_f]$. The dynamics of this sliding surface is given by:

$$\dot{\mathbf{s}}(t) = \mathbf{Z}\dot{\mathbf{E}}\mathbf{V}(t) + \tilde{\lambda}(t)\mathbf{Z}\dot{\mathbf{E}}\mathbf{M}(t) = -\mathbf{a}(t) - \tilde{\lambda}(t)t_{\mathrm{go}}(t)\mathbf{a}(t) \tag{44}$$

This results in the guidance law re-constructed in such a way that the system is always asymptotically driven to the sliding surface, i.e., $\mathbf{s}(t) \to 0$. The rate of convergence corresponds to $\mathrm{e}^{-\tilde{\lambda}(t)t}$ and, when the sliding surface is reached, the system is said to be in sliding phase. The new guidance law can be made as simple as a switching between two states (back or forth towards the sliding surface) and therefore very robust. It is constructed using Lyapunov's direct method by selecting $V(\mathbf{s}) = \frac{1}{2}\mathbf{s}^{\mathrm{T}}(t)\mathbf{s}(t)$ as the candidate Lyapunov function with $V(0) = 0$ and $V(\mathbf{s}) > 0$ for $\mathbf{s}(t) > 0$, as well as imposing:

$$\dot{V}(\mathbf{s}) = \mathbf{s}^{\mathrm{T}}(t)\dot{\mathbf{s}}(t) \leq 0 \tag{45}$$

For the CTVG case, substituting the optimal acceleration (41) into (44) gives:

$$\dot{\mathbf{s}}(t) = -\frac{1}{t_{\mathrm{go}}(t)} K\mathbf{s}(t) \tag{46}$$

where $K = 4$. And in order to satisfy (45), the acceleration input can be augmented, for example, simply as:

$$\mathbf{a}(t) = \frac{6}{t_{\mathrm{go}}^2(t)}\mathbf{ZEM}(t) - \frac{2}{t_{\mathrm{go}}(t)}\mathbf{ZEV}(t) - \frac{\phi}{t_{\mathrm{go}}(t)}\operatorname{sign}\mathbf{s}(t) \tag{47}$$

which gives the following $\dot{\mathbf{s}}(t)$ satisfying now (45):

$$\dot{\mathbf{s}}(t) = -\frac{1}{t_{\mathrm{go}}(t)}\left[K\mathbf{s}(t) + \phi \operatorname{sign}\mathbf{s}(t)\right] \tag{48}$$

Finally, using Lyapunov's second method it can be proven that the algorithm is globally stable when $\phi \geq ||\mathbf{p}(t)|| \; \forall \; t \in [t_0, t_f]$ (Furfaro et al., 2011, 2013b). Moreover, the nonlinear term provides an additional acceleration command, but note that it is only in off-nominal cases. In these cases, the motion is brought inside the sliding surface at the expense of a larger control effort.

To demonstrate the increased robustness of the OSG approach, the CTVG law of Fig. 11 has been augmented with the sliding mode term while reducing the number of waypoints from 14 to only 1. The result is depicted in Fig. 12.

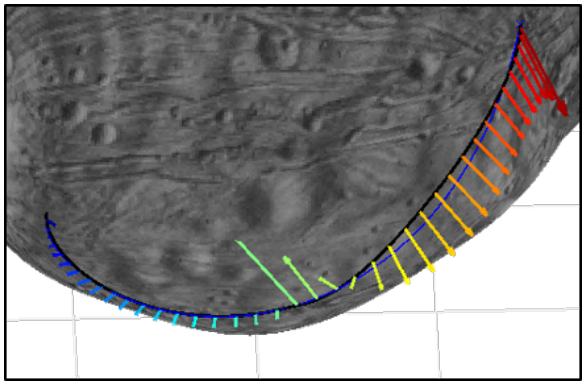

Figure 12: Phobos D&L trajectory using sliding CTVG (arrows represent magnitude and direction of acceleration commands)

Despite relying on a much smaller number of waypoints, the sliding CTVG approach still allows to achieve a successful landing on Phobos, as illustrated by Fig. 12, although presenting slight deviations from the reference trajectory (blue line). However, comparing this figure with Fig. 11, it is observed that the increased robustness comes at the expense of higher and rougher acceleration commands.

The OSG concept can also be extended to the FTVG cases by defining:

$$\mathbf{s}(t) = \mathbf{ZEM}(t) \tag{49}$$

$$\dot{\mathbf{s}}(t) = -t_{\mathrm{go}}(t)\mathbf{a}(t) = -\frac{1}{t_{\mathrm{go}}(t)}K\mathbf{s}(t) \tag{50}$$

with $K = 3$ and modifying the acceleration law (42) to:

$$\mathbf{a}(t) = \frac{3}{t_{\mathrm{go}}^2(t)}\mathbf{ZEM}(t) - \frac{\phi}{t_{\mathrm{go}}(t)}\mathrm{sign}\,\mathbf{s}(t) \tag{51}$$

The main shortcoming of the laws (47) and (51) is that the augmentation with the discontinuous term $\mathrm{sign}\,\mathbf{s}(t)$ can degenerate in the system chattering around the sliding surface, which massively reduces its performance. Such a trend is already noticeable from the comparison between Fig. 11 and 12. To overcome this phenomenon, continuous chattering-free augmentations known as higher-order sliding controllers have been presented over the last years (Furfaro et al., 2013a,

2015). Additional research has also been carried out in the SMC field with its application to increase the robustness of open-loop guidance laws (Orr & Shtessel, 2008, 2009).

3.3. Computational closed-loop guidance

With computational guidance (Special Issue on Computational Guidance and Control, 2017), solutions that minimise equation (33) while meeting desired state and control constraints are computed in real-time. Two classes of algorithms are available to achieve this in a computationally-efficient manner: convex optimisation and pseudospectral methods. These two approaches are described in Sec. 3.3.1 and 3.3.2, respectively.

3.3.1. Convex optimisation

The most relevant mathematical development leading to convex optimisation-based D&L is the reformulation of the trajectory-generation problem into the convex programming framework as a second-order cone program (SOCP), see (Açikmeşe & Ploen, 2005, 2007; Blackmore et al., 2010; Eren et al., 2015) and references therein. To tackle this problem, powerful interior-point solvers exist (Nesterov & Nemirovski, 1994; Sturm, 2002) with guaranteed convergence to the optimal solution of the original problem within a finite number of iterations (for a given neighbourhood around it).

This approach is particularly attractive because it allows the D&L problem to be recast as model predictive control (MPC) (Pascucci et al., 2015) and to solve it very efficiently in real-time (Jerez et al., 2017). Its main difficulty lies in the process of converting non-convex constraints into the convex form, which is known as *lossless convexification*.

There are two sources of non-convexity that are inherent to the trajectory-generation problem: (i) the fuel-depletion dynamics, which have a logarithmic dependence on time; and (ii) thrust magnitude and pointing constraints, due to the norm operator in (12). The first one is directly avoided using the following change of coordinates:

$$z(t) = \ln m(t) \tag{52}$$

while the latter requires the introduction of a surrogate optimisation variable:

$$\Gamma(t) = \frac{\|\mathbf{T}_c(t)\|}{m(t)} \tag{53}$$

A physical illustration of the effect of this surrogate variable is depicted in Fig. 13.

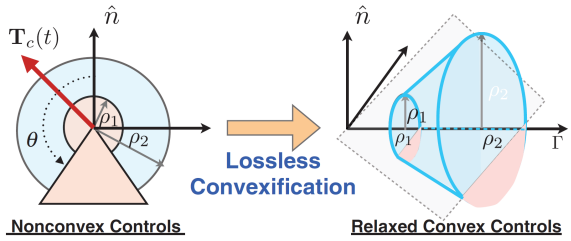

Figure 13: Illustration of the lossless convexification of thrust magnitude and pointing constraints [Source: Eren et al. (2015)]

To solve the D&L problem, the optimisation variables are discretised into N points uniformly spaced by T_S. The objective is then to find a discrete thrust acceleration profile $\mathbf{a}[k]$ ($k \in [1, \cdots, N]$) that minimises fuel consumption, which is equivalent to maximising the final mass of the spacecraft or $z[N]$. The most basic formulation of this problem is provided in SOCP 1 and its main constraints are summarised below:

- Boundary conditions, with $k = 1$ and $k = N$ corresponding to current and touchdown time, t and t_f, respectively. These are the same of Sec. 3.2.3, with the addition that the final thrust acceleration vector $\mathbf{a}[N]$ is required to have no horizontal components;

- Dynamics equations, describing the depletion of fuel and translational motion using a central discretisation scheme with interval T_S. In these equations, α is an engine-dependent constant and the gravity acceleration $\mathbf{g}(t)$ is again assumed uniform;

- Surrogate variable $\Gamma[k]$ and convexification inequality:

$$\|\mathbf{a}[k]\| \leq \Gamma[k] \tag{54}$$

  which becomes an equality once $z[N]$ is maximised;

- Control constraints, consisting of bounded thrust direction and magnitude. The angle between the thrust vector and the vertical direction is constrained by $\tan\theta_{\max}$. The magnitude constraint assumes constant mass $m(t)$ from time t to preserve convexity, which is not restrictive since the actual limits can be re-adjusted via $\{\rho_1,\, \rho_2\}$.

SOCP 1

$$\max_{\mathbf{a},\Gamma} \; z[N], \quad \text{subject to:}$$

Boundary conditions

$$z[1] = \ln m(t), \;\; \mathbf{r}[1] = \mathbf{r}(t), \;\; \mathbf{v}[1] = \mathbf{v}(t), \;\; \mathbf{a}[1] = \mathbf{a}(t)$$

$$\mathbf{r}[N] = \mathbf{r}_f, \;\; \mathbf{v}[N] = \mathbf{v}_f, \;\; \mathbf{a}_{x,y}[N] = 0_{\,2\times 1}, \;\; \mathbf{a}_z[N] \geq 0$$

Dynamics equations, $\quad \forall k \in [1, \cdots, N-1]$

$$z[k+1] = z[k] - \alpha \frac{T_{\mathrm{S}}}{2}\Big(\Gamma[k] + \Gamma[k+1]\Big)$$

$$\mathbf{r}[k+1] = \mathbf{r}[k] + T_{\mathrm{S}}\,\mathbf{v}[k] + \frac{T_{\mathrm{S}}^2}{3}\Big(\mathbf{a}[k] + \frac{\mathbf{a}[k+1]}{2} + \frac{3}{2}\,\mathbf{g}(t)\Big)$$

$$\mathbf{v}[k+1] = \mathbf{v}[k] + \frac{T_{\mathrm{S}}}{2}\Big(\mathbf{a}[k] + \mathbf{a}[k+1] + 2\,\mathbf{g}(t)\Big)$$

Surrogate variable, $\quad \forall k \in [1, \cdots, N]$

$$\|\mathbf{a}[k]\| \leq \Gamma[k]$$

Control constraints, $\quad \forall k \in [1, \cdots, N]$

$$\mathbf{a}_z[k] \geq \frac{\|\mathbf{a}_{x,y}[k]\|}{\tan\theta}$$

$$\frac{\rho_1}{m(t)} \leq \Gamma[k] \leq \frac{\rho_2}{m(t)}$$

The inclusion of additional constraints in this problem is straightforward if they are convex (e.g. subsurface flight avoidance and glideslope limits) or if they can be converted via lossless convexification. If not, a technique known as *successive convexification* can be applied to eliminate any remaining nonlinearities. This approach is based on an iterative process in which non-convex terms are sequentially approximated using information from the previous SOCP solution. To facilitate convergence, a trust region constraint (TRC) is typically imposed between consecutive iterations.

Successive convexification allows to handle certain features that, depending on the target body, may play a critical role for D&L, such as high-order gravitational harmonics, nonlinear aerodynamic forces, non-convex keep-out zones and also free final-time, see (Liu & Lu, 2014; Mao et al., 2016; Lu, 2018) and references therein.

Moreover, this approach effectively enables extending the 3 degree-of-freedom (3-DoF) problem to 6-DoF by incorporating attitude kinematics and decoupling the thrust vector from the attitude of the spacecraft (Szmuk et al., 2017; Szmuk & Açikmeşe, 2018). An alternative approach was proposed in (Lee & Mesbahi, 2015, 2017), which uses piecewise affine (PWA) approximations of the nonlinear 6-DoF dynamics and an MPC formulation with dual quaternions. Its main shortcoming is that, since it relies on PWA approximations, the resolution of the discretised dynamics has a drastic impact on the quality of the obtained solutions.

3.3.2. Pseudospectral methods

An alternative approach to convex optimisation arose with the development of pseudospectral optimal control in (Fahroo & Ross, 2008). Pseudospectral methods allow to transform the infinite-dimensional problem of (33) with state and control constraints into a discrete, finite-dimensional nonlinear programming (NLP) problem, which can be solved using different off-the-shelf solvers. These methods are particularly suitable for aerospace applications due to the guaranteed spectral (i.e. quasi-exponential) convergence of their solution for smooth problems.

With this approach, the cost function, differential equations and constraints are approximated by being defined at a set of discretisation nodes (known as collocation points) and treated as a set of algebraic constraints, in a process called *transcription*. To do so, the physical domain of a variable $t \in [t_0, t_f]$ is converted into a normalised independent variable $\tau \in [-1, 1]$ through the following affine transformation:

$$\tau = \frac{2}{t_f - t_0} t + \frac{t_f + t_0}{t_f - t_0} \tag{55}$$

Different methods can then be employed to compute the location of the collocation points, with one of the simplest corresponding to the roots of a linear combination of Legendre polynomials as follows:

$$(\tau_n)_{i+1} = (\tau_n)_i - \frac{1-\tau_n}{2}\frac{P_{n-1}(\tau_n) + P_n(\tau_n)}{P_{n-1}(\tau_n) - P_n(\tau_n)} \tag{56}$$

with:

$$P_i(\tau) = \prod_{j=0,\, j\neq i}^{N} \frac{\tau - \tau_j}{\tau_i - \tau_j} \tag{57}$$

generating non-uniform grids, where a smaller number of nodes is required to compute a valid solution. Once the domain is discretised, pseudospectral operators for differentiation and integration are also defined. Thanks to the classes of polynomials involved, these operators are more accurate than the standard finite differences for differentiation and trapezoidal rule for integration. Application examples using more sophisticated algorithms, such as the flipped Radau pseudospectral method (RPM), can be found in (Arslantas et al., 2014) and (Sagliano et al., 2017) for lunar landing and Earth re-entry guidance, respectively.

It is important to note that the quality of the obtained solution is strongly dependent on the Jacobian matrix generated from the transcription process. In (Sagliano & Theil, 2013), it is shown how the inherent sparseness of that matrix (due to non-dependencies between states) can be exploited for faster and improved results. Nonetheless, even with a proper transcription, poor scaling of the Jacobian can still lead to numerical difficulties.

Once again, different strategies exist, ranging from *ad hoc* manual scaling, available with widespread pseudospectral tools like DIDO (Elissar, 2015), to more sophisticated self-scaling methods such as Jacobian rows normalisation (JRN) (Rao, 2009) or projected JRN (PJRN) (Sagliano, 2014).

The real-time implementation of pseudospectral optimisation remains a challenging issue because of the NLP problem involved. To tackle this issue, the hybridization of pseudospectral methods and convex optimisation was recently proposed in (Sagliano, 2018). The idea is to combine the more accurate distribution of nodes and pseudospectral operators with the more efficient formulation

and computation of SCOP problems. In that reference, this method was shown to remain real-time capable, while providing improved results compared to the standard convex approach.

3.4. Industrial trends

In terms of technological maturity, the practical applicability of closed-loop techniques (Sec. 3.2 and 3.3) is currently limited, not only due to the restricted number of D&L mission opportunities on small planetary bodies, but essentially because orbit/trajectory control has been conventionally performed by the ground part of the operations and not a direct responsibility of the spacecraft guidance subsystem.

For this reason, the authors believe that, rather than relying on the more elaborate techniques presented in the aforementioned sections, which are still in the realm of research and development, the industrial trend for *short-term* future missions lies on: (i) guidance solutions that combine open-loop trajectories with robust control compensators (recall Sec. 2.2) that have been already proven on attitude control problems; or (ii) simple closed-loop laws, possibly aided by pre-computed trajectory waypoints (recall Fig. 10).

Since the main objective of the project under which this survey was carried out is precisely to increase the maturity and Technology Readiness Level (TRL) of candidate techniques (up to their implementation and validation on a representative environment) for short-term future missions, the remainder of the article is focused on issues that the authors consider central for the improvement and successful implementation of open-loop and traditional closed-loop D&L solutions only.

3.5. Parameterised guidance

The open-loop and traditional closed-loop laws addressed in the survey are summarised in Table 1. Although being directed at the same planetary descent problem (Sec. 2.1), they present quite different properties as highlighted throughout Secs. 3.1 and 3.2.

Table 1: Open-loop and traditional closed-loop laws for planetary descent

Proportional		
PNG	$\mathbf{a}(t) = nV_c(t)\dot{\mathbf{\Lambda}}(t)$	Eq. (20)
APNG	$\mathbf{a}(t) = \frac{n}{t_{\text{go}}^2(t)}\mathbf{ZEM}(t)$	Eq. (24)
Representing the laws as a function of ZEM and ZEV allows to concentrate the knowledge of gravitational forces in these terms		
Predictive and hybrid		
PI	$\Delta\mathbf{v}_S(t) = V_c(t)\frac{\breve{\mathbf{r}}(t_f)}{\breve{r}(t_f)} - \mathbf{v}(t)$	Eq. (27)
KI	$\Delta\mathbf{v}_S(t) = V_c(t)\frac{\breve{\mathbf{r}}(t_f)}{\breve{r}(t_f)} - V_c(t)\left(t_{\text{go}}(t)\dot{\mathbf{\Lambda}}(t) + \mathbf{\Lambda}(t)\right)$	Eq. (31)
Pre-scheduled firings are commanded to generate the required $\Delta\mathbf{v}_S(t)$ and correct the predicted end-of-mission position $\breve{\mathbf{r}}(t_f)$		
Quadratic		
Apollo	$\mathbf{a}(t) = \mathbf{C}_0 + \mathbf{C}_1 t + \mathbf{C}_2 t^2$	Eq. (13)
Open-loop trajectory with closed-form solution as a function of terminal conditions		
Optimal without path constraints		
CTVG	$\mathbf{a}(t) = \frac{6}{t_{\text{go}}^2(t)}\mathbf{ZEM}(t) - \frac{2}{t_{\text{go}}(t)}\mathbf{ZEV}(t)$	Eq. (41)
FTVG	$\mathbf{a}(t) = \frac{3}{t_{\text{go}}^2(t)}\mathbf{ZEM}(t)$	Eq. (42)
Specific constraints may be taken into account but not explicitly enforced, e.g., OFIGL (Ebrahimi et al., 2008) and IACG (Hawkins & Wie, 2011)		
Optimal with path constraints		
Polynomial	$\mathbf{a}(t) = \mathbf{C}_0 + \mathbf{C}_1 t + \ldots + \mathbf{C}_N t^N, \quad N > 2$	Eq. (18)
Open-loop trajectory with optimisation-based solution and possibility to explicitly enforce path constraints		
Nonlinear robust		
Sliding CTVG	$\mathbf{a}(t) = \frac{6}{t_{\text{go}}^2(t)}\mathbf{ZEM}(t) - \frac{2}{t_{\text{go}}(t)}\mathbf{ZEV}(t) - \frac{\phi}{t_{\text{go}}(t)}\text{sign}\,\mathbf{s}(t)$	Eq. (47)
Sliding FTVG	$\mathbf{a}(t) = \frac{3}{t_{\text{go}}^2(t)}\mathbf{ZEM}(t) - \frac{\phi}{t_{\text{go}}(t)}\text{sign}\,\mathbf{s}(t)$	Eq. (51)
Augmentation with nonlinear function, ensuring stability for $\|\|\mathbf{p}(t)\|\| \leq \phi$		

Despite their differences, and from the mindset of using automated tuning methods, it was observed that traditional closed-loop guidance laws shared structural commonalities and could be formalised in terms of LOS kinematics in the following manner:

$$\mathbf{a}(t) = \begin{bmatrix} k_r & k_v \end{bmatrix} V_c(t) \begin{bmatrix} \dfrac{\mathbf{\Lambda}(t)}{t_{\mathrm{go}}(t)} \\ \\ \dot{\mathbf{\Lambda}}(t) \end{bmatrix} - \phi\, \mathbf{h}\left(\mathbf{\Lambda}(t), \dot{\mathbf{\Lambda}}(t), t_{\mathrm{go}}(t)\right) \tag{58}$$

Alternatively, and more sophisticatedly, they can also be parameterised as a function of zero-effort errors:

$$\mathbf{a}(t) = \begin{bmatrix} k_r & k_v \end{bmatrix} \begin{bmatrix} \dfrac{\mathbf{ZEM}(t)}{t_{\mathrm{go}}^2(t)} \\ \\ \dfrac{\mathbf{ZEV}(t)}{t_{\mathrm{go}}(t)} \end{bmatrix} - \phi\, \mathbf{h}\left(\mathbf{ZEM}(t), \mathbf{ZEV}(t), t_{\mathrm{go}}(t)\right) \tag{59}$$

The two equations above clearly show a fixed structure formed by a linear component (parameterised through the gains k_r and k_v) and (optionally) by a nonlinear function $\mathbf{h}(.)$ (weighted by the constant ϕ). As mentioned before, this nonlinear term is introduced to improve robustness properties following the concepts of sliding motion control and it can range from a very simple to a high-order function.

This generalisation is particularly convenient for the application of newly-developed systematic tuning tools (Apkarian & Noll, 2006; Gahinet & Apkarian, 2011), allowing key parameters to be optimised against competing guidance requirements while keeping the rest of the structure fixed. It shall also be remarked that this generalisation does not encapsulate open-loop laws, although these are directly parameterised as time polynomials (18).

Finally, to demonstrate that there might be room for D&L improvement, a parametric analysis of the guidance law shown in Fig. 11 has been performed for a range of guidance gains k_r and k_v (Simplício et al., 2017). Results in terms of touchdown speed and propellant consumption, $V_c(t_f)$ and $\Delta V(t_f)$, are depicted in Fig. 14.

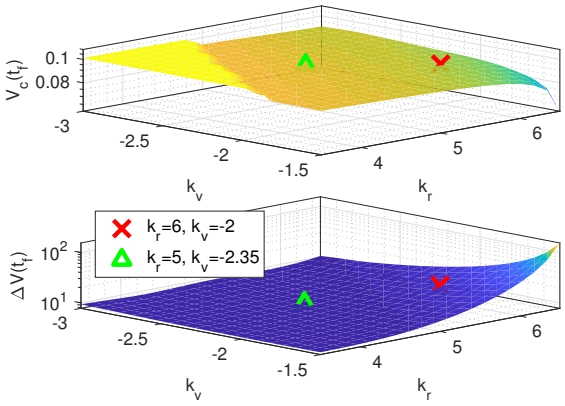

Figure 14: Tuning trade-offs for Phobos D&L using CTVG

This figure provides a clear visualisation of an underlying trade-off between $V_c(t_f)$ and $\Delta V(t_f)$: a choice of gains that minimises touchdown speed will maximise the required ΔV and vice-versa. However, it also shows that the state-of-practice tuning selection of $k_r = 6, k_v = -2$ (marked with $\times$) might not be the most suitable one since choosing, e.g., $k_r = 5, k_v = -2.35$ (marked with $\triangle$), enables a ΔV reduction of 7.1 m/s while only increasing the touchdown speed by 0.003 m/s.

4. Practical Issues

In this final section, the main practical issues identified during this survey are further elaborated. These include the effect of uncertainties on guidance algorithms (Sec. 4.1), the computation of zero-effort errors (Sec. 4.2), as well as the determination of the time-to-go (Sec. 4.3).

4.1. Robustness

Stability and performance characteristics of any real system are affected by many dynamical perturbations or operational uncertainties, ranging from modelling inaccuracies (both deliberate and unknown) to external disturbances. The guidance laws presented in Sec. 3 are typically designed for a single nominal target-spacecraft model, but a successful descent strategy must function properly for all uncertainties within a bounded set. As anticipated in Sec. 3.2.4, pure

optimal guidance laws are more sensitive to uncertainties and perturbations than their robust counterparts, i.e., augmented with sliding mode control (SMC). This section provides a simple illustration of the effect of uncertainties in planetary descent, for the different guidance laws.

The scenario selected to exemplify the uncertainty effect is taken from reference (Hawkins et al., 2010). It simulates a hyper-velocity interception of asteroid Apophis (which will make close approaches to planet Earth in 2029 and 2036) with the interception phase starting at perihelion roughly 1 day before impact. The available thrust force for control is assumed unlimited, but the actuation is switched-off 200 seconds before touch-down. In addition, gravity is assumed constant for ZEM and ZEV computations and all the sensor measurements are assumed ideal. The target asteroid is modelled as a uniform sphere with gravitational coefficient $\mu_T = 15.35$ m^3/s^2 and radius $R_T = 500$ m. Without any guidance actuation, this scenario results in a miss distance of around 40,000 km.

The main source of uncertainty in this type of scenario is known to lie on the gravitational force experienced by the spacecraft due to the irregular and inaccurately known mass distribution of the asteroid and to the proneness of variable third-body perturbations. Thus, a multiplicative uncertainty is introduced around the norm (not direction) of the spacecraft's nominal gravitational acceleration $\mathbf{g}_{S_{\text{nom}}}(\mathbf{r}_T, \mathbf{r}_S)$ assuming a relative uncertainty level $w_g = 100\%$ and where $\Delta_g \in [-1, +1]$ represents the normalised uncertainty (with -1/+1 its minimum/maximum range and 0 its nominal value):

$$\mathbf{g}_S(\mathbf{r}_T, \mathbf{r}_S) = \mathbf{g}_{S_{\text{nom}}}(\mathbf{r}_T, \mathbf{r}_S)\,[1 + w_g \Delta_g] \tag{60}$$

The above uncertainty representation follows the robust control community modelling paradigm known as a linear fractional transformation (LFT). These LFT models are the cornerstone of robust control as they allow capturing the known part of a system and/or variable (in this case $\mathbf{g}_{S_{\text{nom}}}$) and the uncertain component (in (60) the range of Δ_g) in a manner amenable for subsequent robust analysis and control. A detailed description of LFTs is beyond the scope of this survey, but the interested reader is referred to (Doyle et al., 1991; Zhou

et al., 1995) and references therein. Their use in Space for robust stability and performance analysis of different systems is now prevalent (Bourdon et al., 2002; Charbonnel, 2010; Simplício et al., 2016) and as part of the UK Space Agency project these techniques are also introduced for the D&L problem.

Simulations are depicted for a fixed set of 20 values of Δ_g for the CTVG law (terminal velocity constrained to 0 m/s, i.e., soft landing) in Fig. 15 and for the FTVG law (free terminal velocity) in Fig. 16.

Both figures show the outcome of the two (pure) optimal laws (gray lines) against their SMC-augmented (robust) counterparts (red lines) – for the latter a constant $\phi = 200$ is used. The same end-of-mission time is commanded for all the cases. The nominal responses, i.e. $\Delta_g = 0$, are also shown (black lines). The main difference between the CTVG and the FTVG laws is related to the reduction of velocity towards 0 m/s imposed by the former (Fig. 15b vs. 16b). As expected, this manoeuvre is more demanding in terms of control acceleration (Fig. 15d vs. 16d). Note also that the linear dependence on time anticipated for the pure optimal laws from (37) is also easily seen.

For the pure optimal laws, it is also observed that off-nominal spacecraft's gravitational accelerations lead to significantly dispersed trajectories (see Figs. 15a and 16a for the heliocentric frame, and Figs. 15c and 16c for the relative frame). This effect is therefore reflected into a degradation of the landing accuracy. Furthermore, the FTVG law, by employing only position information (42), shows larger sensitivity to uncertainties, which even causes the spacecraft to miss the asteroid for $|\Delta_g| \geq 0.8$ (in other words, the robust laws improve against gravity uncertainty of at least 80% larger in norm-size). After augmenting the guidance schemes with SMC, and although the trajectory is still affected by the presence of uncertainties, its degradation is reduced to approximately half for both laws (Figs. 15c and 16c). Of course, this comes at the expense of a significantly higher actuation effort (Figs. 15d and 16d) for off-nominal cases. This decrease in sensitivity and consequent increase in actuation effort is a critical trade-off often encountered in aerospace systems, in which better robustness properties are attained through a compromise in terms of optimality.

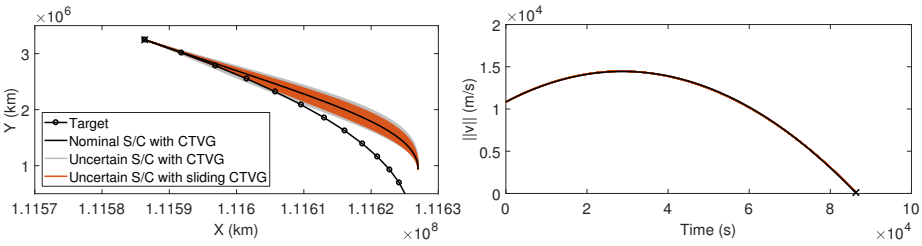

(a) Heliocentric position (b) Closing velocity

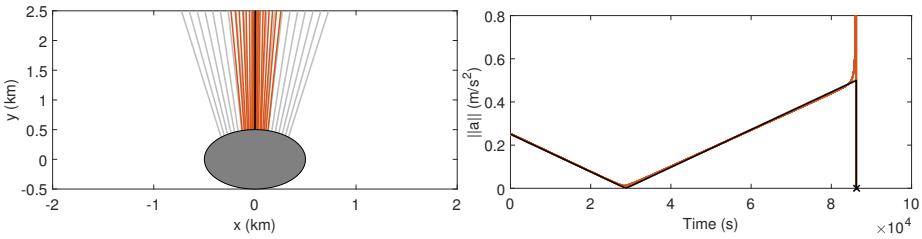

(c) Relative position (d) Control acceleration norm

Figure 15: Robustness of CTVG laws (with $\mathbf{v}_f = 0$)

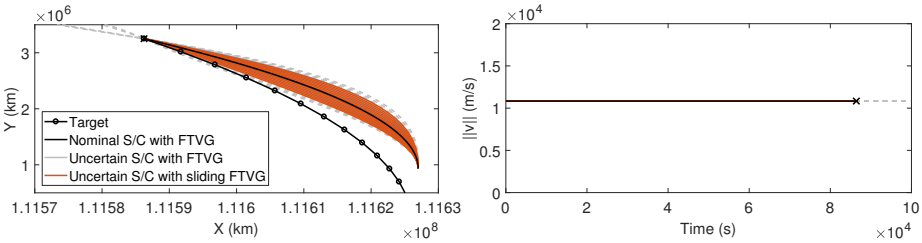

(a) Heliocentric position (b) Closing velocity

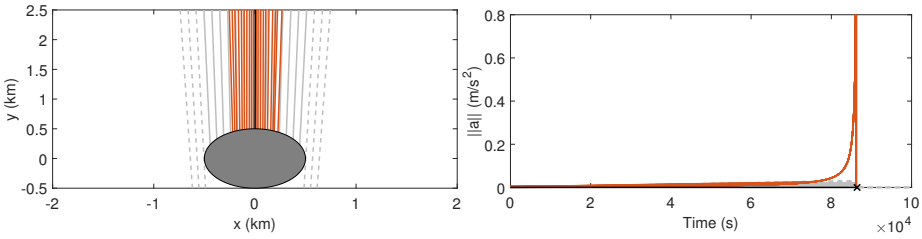

(c) Relative position (d) Control acceleration norm

Figure 16: Robustness of FTVG laws (dashed lines indicate missed interceptions)

As a potential axis for improvement, and as briefly mentioned before, the robust control community has particularly well suited methods and tools to systematically address the aforementioned type of trade-offs, explicitly considering the effect of uncertainties and disturbances. As previously shown, these uncertainties can be modelled as time-invariant LFTs, but this formalism also allows to indirectly capture time-varying effects via linear parameter-varying (LPV) models (details on LPV modelling can be found in (Marcos & Bennani, 2009) and references therein). Furthermore, and also favoured by the use of the robust control framework, recent automated tuning tools (Apkarian & Noll, 2006; Gahinet & Apkarian, 2011) have appeared that will be able to exploit the parameterisation of the guidance laws proposed in (58) and (59) – or facilitate the synthesis of control compensators that minimise orbital perturbations with respect to a reference trajectory (Simplício et al., 2018a).

4.2. Zero-effort errors computation

In Sec. 3.2 it was shown that defining guidance laws as a function of the zero-effort errors allows to gather the effects of an inaccurate knowledge of the gravitational environment in the value of ZEM and ZEV (and these effects were exemplified in Sec. 4.1). For this reason, it is important to compute the ZEM and ZEV (and therefore the integrations in (10)) as accurately as possible. To do so, the following options exist in the literature:

- If the gravitational force is not significant, then it can be neglected for ZEM and ZEV computations;
- If the gravitational force is slowly changing during the manoeuvre, it can be assumed constant, yielding:

$$\begin{aligned} \mathbf{ZEM}(t) &= \mathbf{r}_f - \left[\mathbf{r}(t) + t_{\text{go}}(t)\mathbf{v}(t) + \frac{1}{2}t_{\text{go}}^2(t)\mathbf{g}\right] \\ \mathbf{ZEV}(t) &= \mathbf{v}_f - \left[\mathbf{v}(t) + t_{\text{go}}(t)\mathbf{g}\right] \end{aligned} \tag{61}$$

- For a fast but more accurate computation, the value of ZEM and ZEV can be estimated from the linearised time-varying state transition matrix (refer to (Battin, 1987) for more details);

- Ultimately, the value of ZEM and ZEV can be computed from the full numerical propagation of the equations of motion (3).

The options above are organised in increasing levels of accuracy. However, it shall be remarked that more accurate approaches are also associated with higher computational needs.

4.3. Time-to-go determination

Most of the guidance laws presented in this article are implemented as a function of the time-to-go t_{go} (or, alternatively, the end-of-mission time t_f). Therefore, it is convenient to have ways of systematically setting an appropriate time-to-go throughout the mission. A first option is to specify t_{go} as dependent on additional criteria. For example, for the Apollo guidance law, t_{go} is selected so that the vertical component of the spacecraft acceleration is a linear function of time (Ploen et al., 2006).

However, the performance of guidance algorithms can be significantly improved by choosing the value of t_{go} so as to achieve optimal propellant consumption. Hence, a generic option is to execute a line search over $t_{\text{go}} \in \left[t_{\text{go}_{\text{MIN}}}, t_{\text{go}_{\text{MAX}}}\right]$ for each initial state in order to minimise the cost function (Ploen et al., 2006):

$$J(t_{\text{go}}) = \frac{1}{2}\int_{t}^{t+t_{\text{go}}} \mathbf{a}^{\text{T}}(\tau)\mathbf{a}(\tau)\,\mathrm{d}\tau \tag{62}$$

The lower bound $t_{\text{go}_{\text{MIN}}}$ is given by physical constraints such as maximum thrust capability or allowed acceleration, while the upper bound $t_{\text{go}_{\text{MAX}}}$ depends typically on mission specifications such as acceptable duration.

In addition, using the optimal guidance laws of Sec. 3.2.3, the optimal t_{go} must render the Hamiltonian constant over the optimal trajectory:

$$H(\mathbf{x}(t), \mathbf{a}(t))|_{\text{optimal}} = 0 \tag{63}$$

Therefore, for a mission using the CTVG, substituting (41) into (38) and assuming constant gravity (Guo et al., 2011), the optimal t_{go} can be determined numerically (or analytically if the gravity field $\mathbf{g}$ is negligible) by solving:

$$\begin{aligned} t_{\text{go}}^4\mathbf{g}^{\text{T}}\mathbf{g} - 2t_{\text{go}}^2\left(\mathbf{v}^{\text{T}}\mathbf{v} + \mathbf{v}_f^{\text{T}}\mathbf{v} + \mathbf{v}_f^{\text{T}}\mathbf{v}_f\right) + \\ + 12t_{\text{go}}\left(\mathbf{r}_f - \mathbf{r}\right)^{\text{T}}\left(\mathbf{v}_f + \mathbf{v}\right) - 18\left(\mathbf{r}_f - \mathbf{r}\right)^{\text{T}}\left(\mathbf{r}_f - \mathbf{r}\right) = 0 \end{aligned} \tag{64}$$

The same can be performed for FTVG laws but in this case substituting (42) into (38):

$$t_{\mathrm{go}}^4 \mathbf{g}^{\mathrm{T}}\mathbf{g} - 4t_{\mathrm{go}}^2 \left[\mathbf{v}^{\mathrm{T}}\mathbf{v} - (\mathbf{r}_f - \mathbf{r})^{\mathrm{T}}\mathbf{g}\right] + 16 t_{\mathrm{go}} (\mathbf{r}_f - \mathbf{r})^{\mathrm{T}}\mathbf{v} - 12 (\mathbf{r}_f - \mathbf{r})^{\mathrm{T}}(\mathbf{r}_f - \mathbf{r}) = 0 \tag{65}$$

Finally, it shall be noted that the laws (58) and (59) become singular when $t \to t_f$ (i.e., $t_{\mathrm{go}}(t) \to 0$), which must be prevented. The most simple way to do it is by switching-off the actuation immediately before the end-of-mission. The exact instant of time is computed as a trade-off between allowable zero-effort errors and maximum acceleration capability.

5. Conclusions

This article reviews and analyses the state-of-the-art in guidance techniques as applied to the Space field, mainly for planetary interception and/or descent missions. The usefulness of this survey is related to the fact that important developments on distinct scientific fields often take place independently and in here a coherent presentation framework has been adopted to facilitate interdisciplinary cross-pollination towards effective planetary descent techniques. Most notably, this framework gathers technological developments from Control Theory and Space Mission Analysis (Sec. 2.2) as applied to landing on small and larger planetary bodies (Sec. 2.3).

The guidance laws surveyed in this paper present very different properties. Proportional laws, and their evolutions based on optimal control theory, are by far the most widespread techniques when it comes to landing on small bodies. But recently, their robustness properties have been improved against dynamical perturbations and uncertainties by employing results from nonlinear sliding mode control (at the expense of additional control effort). On the other hand, predictive and hybrid approaches allow to reduce the overall control effort via pulsed navigation, but are less accurate since they rely on a linearised propagation of the system states. In parallel, notable advancements have taken place since the Apollo program on explicitly constrained trajectories, being most commonly

targeted at larger bodies using very efficient optimisation frameworks. Despite these differences, it was shown that traditional closed-loop techniques share structural commonalities that are particularly convenient for the application of tuning methods against competing requirements.

In addition, this survey article has presented an evaluation of the key practical issues for deployment of these guidance laws. For example, it was shown (Sec. 4.1) that special care must be devoted to ensure robustness of autonomous descent systems on extremely variable and uncertain environments, which are characteristic of planetary bodies with irregular shapes and mass distributions. This requires the ability to effectively model and account for these uncertain effects when synthesising guidance and control algorithms. These issues are addressed within the UK Space Agency project under which this survey was developed for the case of a future descent and landing in Phobos.

References

Açikmeşe, B., Aung, M., Casoliva, J., Mohan, S., Johnson, A., Scharf, D., Masten, D., Scotkin, A., Wolf, S., & Regehr, M. (2013). Flight Testing of Trajectories Computed by G-FOLD. In *The 23rd AAS/AIAA Spacefilght Mechanics Meeting*. Kauai, HI.

Açikmeşe, B., & Ploen, S. (2005). A Powered Descent Guidance Algorithm for Mars Pinpoint Landing. In *The 2005 AIAA Guidance, Navigation, and Control Conference*. San Franciso, CA.

Açikmeşe, B., & Ploen, S. (2007). Convex Programming Approach to Powered Descent Guidance for Mars Landing. *Journal of Guidance, Control, and Dynamics*, *30*, 1353–1366.

Apkarian, P., & Noll, D. (2006). Nonsmooth $\mathcal{H}_\infty$ Synthesis. *Transactions on Automatic Control*, *51*, 71–86.

Arslantas, Y., Oehlschlägel, T., Sagliano, M., Theil, S., & Braxmaier, C. (2014). Safe Landing Area Determination for a Moon Lander by Reachability Analysis. In *The 65th International Astronautical Congress*. Toronto, Canada.

Barraclough, S., Ratcliffe, A., Buchwald, R., Chapuy, M., Garland, M., & Rebuffat, D. (2014). Phootprint: A European Phobos Sample Return Mission. In *The 11th International Planetary Probe Workshop*. Passadena, CA.

Battin, R. (1987). *An Introduction to the Mathematics and Methods of Astrodynamics*. (1st ed.). AIAA Education Series.

Bhaskaran, S., Mastrodemos, N., Riedel, J., & Synnott, S. (2004). Optical Navigation for the STARDUST Wild 2 Encounter. In *The 18th International Symposium on Space Flight Dynamics*. Munich, Germany.

Blackmore, L. (2016). Autonomous Precision Landing of Space Rockets. *The Bridge on Frontiers of Engineering*, *4*, 15–20.

Blackmore, L., Açikmeşe, B., & Scharf, D. (2010). Minimum-Landing-Error Powered-Descent Guidance for Mars Landing Using Convex Optimization. *Journal of Guidance, Control, and Dynamics*, *33*, 1161–1171.

Bourdon, J., Delpy, P., Ganet, M., Quinquis, I., & Ankersen, F. (2002). Application of $\mathcal{H}_\infty$ Design on ATV Control Loop During the Rendezvous Phase. In *The 5th ESA International Conference on Spacecraft Guidance, Navigation and Control Systems*. Frascati, Italy.

Charbonnel, C. (2010). $\mathcal{H}_\infty$ Controller Design and μ-Analysis: Powerful Tools for Flexible Satellite Attitude Control. In *The 2010 AIAA Guidance, Navigation, and Control Conference*. Toronto, Canada.

Doyle, J., Packard, A., & Zhou, K. (1991). Review of LFTs, LMIs and μ. In *The 30th IEEE Conference on Decision and Control*. Brighton, UK.

D'Souza, C. (1997). An optimal guidance law for planetary landing. In *The 1997 AIAA Guidance, Navigation, and Control Conference*. New Orleans, LA.

Ebrahimi, B., Bahrami, M., & Roshanian, J. (2008). Optimal sliding-mode guidance with terminal velocity constraint for fixed-interval propulsive maneuvers. *Acta Astronautica*, *62*, 556–562.

Elissar (2015). *Description of DIDO Optimal Control Software*. `http://www.elissarglobal.com/`.

Eren, U., Dueri, D., & Açikmeşe, B. (2015). Constrained Reachability and Controllability Sets for Planetary Precision Landing via Convex Optimization. *Journal of Guidance, Control, and Dynamics*, *38*, 2067–2083.

Fahroo, F., & Ross, M. (2008). Pseudospectral Methods for Infinite-Horizon Optimal Control Problems. *Journal of Guidance, Control, and Dynamics*, *31*, 927–936.

Falcoz, A., Pittet, C., Bennani, S., Guignard, A., Bayart, C., & Frapard, B. (2015). Systematic design methods of robust and structured controllers for satellites. *Space Journal*, *7*, 319–334.

Ferrari, F., Lavagna, M., Scheper, M., Burmann, B., & Carnelli, I. (2015). The European Asteroid Impact Mission: Phase A Design and Mission Analysis. In *The 2015 AAS/AIAA Astrodynamics Specialist Conference*. Vail, CO.

Furfaro, R., Cersosimo, D., & Wibben, D. (2013a). Asteroid Precision Landing via Multiple Sliding Surfaces Guidance Techniques. *Journal of Guidance, Control, and Dynamics*, *36*, 1075–1092.

Furfaro, R., Gaudet, B., Wibben, D., & Simo, J. (2013b). Development of Nonlinear Guidance Algorithms for Asteroids Close-Proximity Operations. In *The 2013 AIAA Guidance, Navigation, and Control Conference*. Boston, MA.

Furfaro, R., Selnick, S., Cupples, M., & Cribb, M. (2011). Nonlinear Sliding Guidance Algorithms for Precision Lunar Landing. In *The 2011 AAS/AIAA Spaceflight Mechanics Meeting*. New Orleans, LA.

Furfaro, R., Wibben, D., Gaudet, B., & Simo, J. (2015). Terminal Multiple Surface Sliding Guidance for Planetary Landing. *Journal of the Astronautical Sciences*, *62*, 73–99.

Gahinet, P., & Apkarian, P. (2011). Structured $\mathcal{H}_\infty$ Synthesis in MATLAB. In *The 18th IFAC World Congress*. Milan, Italy.

Geurts, K., Fantinati, C., Ulamec, S., & Willnecker, R. (2014). Rosetta Lander: On-Comet Operations Preparation and Planning. In *The AIAA SpaceOps 2014 Conference*. Passadena, CA.

Gil-Fernandez, J., Panzeca, R., & Corral, C. (2008). Impacting Small Near Earth Objects. *Advances in Space Research*, *42*, 1352–1363.

Guo, Y., Hawkins, M., & Wie, B. (2011). Optimal Feedback Guidance Algorithms for Planetary Landing and Asteroid Intercept. In *The 2011 AAS/AIAA Astrodynamics Specialist Conference*. Girdwood, AK.

Guo, Y., Hawkins, M., & Wie, B. (2012). Waypoint-Optimized Zero-Effort-Miss/Zero-Effort-Velocity Feedback Guidance for Mars Landing. In *The 2012 AAS/AIAA Spaceflight Mechanics Meeting*. Charleston, SC.

Guo, Y., Hawkins, M., & Wie, B. (2013). Applications of Generalized Zero-Effort-Miss/Zero-Effort-Velocity Feedback Guidance Algorithm. *Journal of Guidance, Control, and Dynamics*, *36*, 810–820.

Hawkins, M., Guo, Y., & Wie, B. (2011). Guidance algorithms for asteroid intercept missions with precision targeting requirements. In *The 2011 AAS/AIAA Astrodynamics Specialist Conference*. Girdwood, AK.

Hawkins, M., Guo, Y., & Wie, B. (2012). Spacecraft Guidance Algorithms for Asteroid Intercept and Rendezvous Missions. *International Journal of Aeronautical and Space Sciences*, *13*, 154–169.

Hawkins, M., Pitz, A., & Wie, B. (2010). Terminal-Phase Guidance and Control Analysis of Asteroid Interceptors. In *The 2010 AIAA Guidance, Navigation, and Control Conference*. Toronto, Canada.

Hawkins, M., & Wie, B. (2011). Impact-Angle Control of Asteroid Interceptors/Penetrators. In *The 2011 AAS/AIAA Spaceflight Mechanics Meeting*. New Orleans, LA.

Jerez, J., Merkli, S., Bennani, S., & Strauch (2017). FORCES-RTTO: A Tool for On-board Real-time Autonomous Trajectory Planning. In *The 10th*

International ESA Conference on Guidance, Navigation and Control Systems. Salzburg, Austria.

Joffre, E., Zamaro, M., Silva, N., Marcos, A., Simplício, P., & Richardson, B. (2017). Landing on Small Bodies Trajectory Design, Robust Nonlinear Guidance and Control. In *The 27th AAS/AIAA Spacefilght Mechanics Meeting*. San Antonio, TX.

Kim, B., Lee, G., & Han, H. (1998). Biased PNG law for impact with angular constraint. *Transactions on Aerospace and Electronic Systems*, *34*, 277–288.

Klumpp, A. (1974). Apollo lunar descent guidance. *Automatica*, *10*, 133–146.

Kubitschek, D. (2003). Impactor spacecraft targeting for the Deep Impact mission to comet Temple 1. In *The 2003 AAS/AIAA Astrodynamics Specialist Conference*. Big Sky, MT.

Kuninaka, H., & Hayabusa-2 team (2015). Deep Space Exploration of Hayabusa-2 Spacecraft. In *The 30th International Symposium on Space Technology and Science*. Kobe, Japan.

Lara, M., & Scheeres, D. (2003). Stability bounds for three-dimensional motion close to asteroids. *Journal of the Astronautical Sciences*, *50*, 389–409.

Lee, U., & Mesbahi, M. (2015). Optimal Powered Descent Guidance with 6-DoF Line of Sight Constraints via Unit Dual Quaternions. In *The AIAA SciTech 2015 Forum*. Kissimmee, FL.

Lee, U., & Mesbahi, M. (2017). Constrained Autonomous Precision Landing via Dual Quaternions and Model Predictive Control. *Journal of Guidance, Control, and Dynamics*, *40*, 292–308.

Levant, A. (2007). Principles of 2-sliding mode design. *Automatica*, *43*, 576–586.

Li, S., & Jiang, X. (2014). Review and prospect of guidance and control for Mars atmospheric entry. *Progress in Aerospace Sciences*, *69*, 40–57.

Liu, X., & Lu, P. (2014). Solving Nonconvex Optimal Control Problems by Convex Optimization. *Journal of Guidance, Control, and Dynamics*, *37*, 750–765.

Lu, P. (2018). Propellant-Optimal Powered Descent Guidance. *Journal of Guidance, Control, and Dynamics*, *41*, 813–826.

Lunghi, P., Lavagna, M., & Armellin, R. (2013). Semi-Analytical Adaptive Guidance Algorithm for Fast Retargeting Maneuvers Computation During Planetary Descent and Landing. In *The 12th Symposium on Advanced Space Technologies in Robotics and Automation*. Noordwijk, Netherlands.

Lunghi, P., Lavagna, M., & Armellin, R. (2014). Semi-analytical guidance algorithm for autonomous close approach to non-cooperative low-gravity targets. In *The 2014 AAS/AIAA Spaceflight Mechanics Meeting*. Santa Fe, NM.

Mao, Y., Szmuk, M., & Açikmeşe, B. (2016). Successive Convexification of Non-Convex Optimal Control Problems and Its Convergence Properties. In *The 55th IEEE Conference on Decision and Control*. Las Vegas, NV.

Marcos, A., & Bennani, S. (2009). LPV Modeling, Analysis and Design in Space Systems: Rationale, Objectives and Limitations. In *The 2009 AIAA Guidance, Navigation, and Control Conference*. Chicago, IL.

Nesterov, Y., & Nemirovski, A. (1994). *Interior-Point Polynomial Algorithms in Convex Programming*. (1st ed.). SIAM.

Orr, J., & Shtessel, Y. (2008). Robust Control of Lunar Spacecraft Powered Descent Using a Second Order Sliding Mode Technique. In *The 2008 AIAA Guidance, Navigation, and Control Conference and Exhibit*. Honolulu, HI.

Orr, J., & Shtessel, Y. (2009). Robust Lunar Spacecraft Autopilot Design Using High-Order Sliding Mode Control. In *The 2009 AIAA Guidance, Navigation, and Control Conference*. Chicago, IL.

Pascucci, A., Bennani, S., & Bemporad, A. (2015). Model Predictive Control

for Powered Descent Guidance and Control. In *The 2015 European Control Conference*. Linz, Austria.

Ploen, S., Açikmeşe, B., & Wolf, A. (2006). A Comparison of Powered Descent Guidance Laws for Mars Pinpoint Landing. In *The 2006 AIAA/AAS Astrodynamics Specialist Conference and Exhibit*. Keystone, CO.

Rao, A. V. (2009). A Survey of Numerical Methods for Optimal Control. In *The 2009 AAS/AIAA Astrodynamics Specialist Conference*. Pittsburgh, PA.

Sagliano, M. (2014). Performance analysis of linear and nonlinear techniques for automatic scaling of discretized control problems. *Operations Research Letters*, *42*, 231–216.

Sagliano, M. (2018). Pseudospectral Convex Optimization for Powered Descent and Landing. *Journal of Guidance, Control, and Dynamics*, *41*, 320–334.

Sagliano, M., & Theil, S. (2013). Hybrid Jacobian Computation for Fast Optimal Trajectories Generation. In *The 2013 AIAA Guidance, Navigation, and Control Conference*. Boston, MA.

Sagliano, M., Theil, S., D'Onofrio, V., & Bergsma, M. (2017). SPARTAN: A Novel Pseudospectral Algorithm for Entry, Descent, and Landing Analysis. In *The 4th CEAS EuroGNC Conference*. Warsaw, Poland.

Scharf, D., Regehr, M., Vaughan, G., Benito, J., Ansari, H., Aung, M., Johnson, A., Casoliva, J., Mohan, S., Dueri, D., Açikmeşe, B., Masten, D., & Nietfeld, S. (2014). ADAPT Demonstrations of Onboard Large-Divert Guidance with a VTVL Rocket. In *The 2014 IEEE Aerospace Conference*. Passadena, CA.

Shtessel, Y., Edwards, C., Fridman, C., & Levant, A. (2014). *Sliding Mode Control and Observation*. (1st ed.). Birkhäuser.

Simplício, P., Bennani, S., Marcos, A., Roux, C., & Lefort, X. (2016). Structured Singular-Value Analysis of the Vega Launcher in Atmospheric Flight. *Journal of Guidance, Control, and Dynamics*, *39*, 1342–1355.

Simplício, P., Marcos, A., Joffre, E., Zamaro, M., & Silva, N. (2017). Parameterised Laws for Robust Guidance and Control of Planetary Landers. In *The 4th CEAS EuroGNC Conference*. Warsaw, Poland.

Simplício, P., Marcos, A., Joffre, E., Zamaro, M., & Silva, N. (2018a). Synthesis and analysis of robust control compensators for Space descent & landing. *International Journal of Robust and Nonlinear Control*, *28*, 3871–3892.

Simplício, P., Marcos, A., Joffre, E., Zamaro, M., & Silva, N. (2018b). Systematic Performance-oriented Guidance Tuning for Descent & Landing on Small Planetary Bodies. *Acta Astronautica, Special Issue on EUCASS 2017 System & GNC*, *in press*.

Singh, G., SanMartin, A., & Wong, E. (2007). Guidance and Control Design for Powered Descent and Landing on Mars. In *The 2007 IEEE Aerospace Conference*. Big Sky, MT.

Special Issue on Computational Guidance and Control (2017). *Journal of Guidance, Control, and Dynamics*, *40*.

Sturm, J. (2002). Implementation of Interior Point Methods for Mixed Semidefinite and Second Order Cone Optimization Problems. *Optimization Methods and Software*, *17*, 1105–1154.

Szmuk, M., & Açikmeşe, B. (2018). Successive Convexification for 6-DoF Mars Rocket Powered Landing with Free-Final-Time. In *The AIAA SciTech 2018 Forum*. Kissimmee, FL.

Szmuk, M., Eren, U., & Açikmeşe, B. (2017). Successive Convexification for Mars 6-DoF Powered Descent Landing Guidance. In *The AIAA SciTech 2017 Forum*. Grapevine, TX.

Wie, B. (2008). *Space Vehicle Dynamics and Control*. (2nd ed.). AIAA Education Series.

Williams, B., Antreasian, P., Carranza, E., Jackman, C., Leonard, J., Nelson, D., Page, B., Stanbridge, D., Wibben, D., Williams, K., Moreau, M., Berry,

K., Getzandanner, K., Liounis, A., Mashiku, A., Highsmith, D., Sutter, B., & Lauretta, D. (2018). OSIRIS-REx Flight Dynamics and Navigation Design. *Space Science Reviews*, *214*.

Wong, E., Singh, G., & Masciarelli, J. (2006). Guidance and Control Design for Hazard Avoidance and Safe Landing on Mars. *Journal of Spacecraft and Rockets*, *43*, 378–384.

Yoshimitsu, T., Kawaguchi, J., Hashimoto, T., Kubota, T., Uo, M., Morita, H., & Shirakawa, K. (2009). Hayabusa – final autonomous descent and landing based on target marker tracking. *Acta Astronautica*, *65*, 657–665.

Zarchan, P. (1994). *Tactical and Strategic Missile Guidance*. (2nd ed.). AIAA Progress in Astronautics and Aeronautics.

Zhang, J., Dauphas, N., Davis, A., & Fedkin, A. (2012). The proto-Earth as a significant source of lunar material. *Nature Geoscience*, *5*, 251–255.

Zhou, K., Doyle, J., & Glover, K. (1995). *Robust and Optimal Control*. (1st ed.). Prentice-Hall.

Zhou, L., & Xia, Y. (2014). Improved ZEM/ZEV feedback guidance for Mars powered descent phase. *Advances in Space Research*, *54*, 2446–2455.